To cite this article: María Jazmín Abraham-Juárez, Amanda Schrager-Lavelle, Jarrett Man, Clinton Whipple, Pubudu Handakumbura, Courtney Babbitt, Madelaine Bartlett, Evolutionary Variation in MADS Box Dimerization Affects Floral Development and Protein Abundance in Maize, *The Plant Cell*, Volume 32, Issue 11, November 2020, Pages 3408–3424, https://doi.org/10.1105/tpc.20.00300

The Plant Cell, Vol. 32: 3408–3424, November 2020, www.plantcell.org © 2020 ASPB.

BREAKTHROUGH REPORT

Evolutionary Variation in MADS Box Dimerization Affects Floral Development and Protein Abundance in Maize[OPEN]

María Jazmín Abraham-Juárez,[a,b,1] Amanda Schrager-Lavelle,[a,c,1] Jarrett Man,[a] Clinton Whipple,[d] Pubudu Handakumbura,[a,e] Courtney Babbitt,[a] and Madelaine Bartlett[a,2]

[a] Biology Department, University of Massachusetts, Amherst, 01003 Massachusetts
[b] CONACYT-Instituto Potosino de Investigación Científica y Tecnológica A.C., 78216 San Luis Potosi, Mexico
[c] Biology Department, Colorado Mesa University, Grand Junction, 81501 Colorado
[d] Biology Department, Brigham Young University, Provo, 84602 Utah
[e] Pacific Northwest National Laboratory, Richland, 99354 Washington

Interactions between MADS box transcription factors are critical in the regulation of floral development, and shifting MADS box protein-protein interactions are predicted to have influenced floral evolution. However, precisely how evolutionary variation in protein-protein interactions affects MADS box protein function remains unknown. To assess the impact of changing MADS box protein-protein interactions on transcription factor function, we turned to the grasses, where interactions between B-class MADS box proteins vary. We tested the functional consequences of this evolutionary variability using maize (*Zea mays*) as an experimental system. We found that differential B-class dimerization was associated with subtle, quantitative differences in stamen shape. In contrast, differential dimerization resulted in large-scale changes to downstream gene expression. Differential dimerization also affected B-class complex composition and abundance, independent of transcript levels. This indicates that differential B-class dimerization affects protein degradation, revealing an important consequence for evolutionary variability in MADS box interactions. Our results highlight complexity in the evolution of developmental gene networks: changing protein-protein interactions could affect not only the composition of transcription factor complexes but also their degradation and persistence in developing flowers. Our results also show how coding change in a pleiotropic master regulator could have small, quantitative effects on development.

INTRODUCTION

Floral organ morphology is diverse, but the master regulators controlling floral organ development are conserved. Many of the master regulators controlling floral organ development are transcription factors encoded by the ABC(DE) genes. The ABC(DE) model proposes how these transcription factors act together to regulate the development of floral organs. All but one of the original ABC(DE) genes encode MADS box transcription factors (reviewed in Krizek and Fletcher, 2005). Although derived from analyses of genetic mutants in the eudicots *Antirrhinum majus* and Arabidopsis (*Arabidopsis thaliana*), some aspects of the ABC(DE) model can explain the genetics of floral development in distantly related angiosperms. For example, B-class gene function is deeply conserved. B-class genes regulate stamen and petal development in many angiosperms, even when petal and stamen homologs are highly modified (reviewed in Litt and Kramer, 2010). How, then, can floral organs vary so extensively in form and function when they are specified by orthologous genes?

The combinatorial assembly of MADS box protein complexes provides a framework to answer this question, in the floral quartet model (Theissen and Saedler, 2001; Theissen et al., 2016). MADS box proteins may function as tetramers or "floral quartets," with tetramer composition determining DNA binding and downstream gene regulation. For example, tetramers of B-, C-, and E-class proteins (BCE complexes) likely specify Arabidopsis stamen identity, and tetramers of C- and E-class proteins likely specify carpel identity (Honma and Goto, 2001; Theissen and Saedler, 2001; Theissen et al., 2016). Evidence for the floral quartet model includes genetic data, in vitro characterization of protein-protein interactions, and in planta evidence for MADS box complex formation and DNA binding, particularly in Arabidopsis (reviewed in Theissen et al., 2016). Beyond Arabidopsis, the paralogs available to form MADS box complexes differ between lineages, but general classes of interactions are conserved. For example, B-class genes have complex histories of lineage-specific duplications, but most B-class paralogs participate in BCE complexes in vitro (Veron et al., 2007; Zhang et al., 2018). This conservation of protein-protein interactions, coupled to the functional conservation of many MADS box genes, suggests that complexes of homologous MADS box proteins specify homologous floral organs in different lineages. Mixing and matching of MADS box paralogs in these

[1] These authors contributed equally to this work.
[2] Address correspondence to mbartlett@umass.edu.
The author responsible for distribution of materials integral to the findings presented in this article in accordance with the policy described in the Instructions for Authors (www.plantcell.org) is: Madelaine Bartlett (mbartlett@umass.edu).
[OPEN]Articles can be viewed without a subscription.
www.plantcell.org/cgi/doi/10.1105/tpc.20.00300

IN A NUTSHELL

Background. The regulatory network that controls floral organ formation is complex and still not completely understood. This network has also been changing over the course of evolution, leading to immense floral diversity. MADS-box transcription factors are important regulators of floral organ development, and changing interactions between MADS-box proteins are predicted to have influenced floral evolution. However, the functional consequences of evolutionary change to MADS-box protein-protein interactions were unknown. Grasses are an excellent family to explore these consequences due to high genetic diversity, evolutionary variation in MADS-box protein-protein interactions, and the numerous genetic model systems in the family. We used the genetic and genomic resources available in maize to determine the functional consequences of evolutionary variation in dimerization of a key regulator of floral development, STERILE TASSEL SILKY EAR1 (STS1).

Question. STS1 dimerization varies across the grasses. In this work, we set out to discover the effect of some of this evolutionary variation on floral development, downstream gene expression and protein complex assembly in maize.

Findings. We found that evolutionary variants of STS1 differentially affect downstream gene expression and protein complex assembly in maize. Surprisingly, we found that STS1 dimerization changed protein degradation dynamics, which had not been described. This discovery adds a new layer of complexity to the regulation of flower development, and how that regulation changes over deep time. We also found that a coding change to *STS1*, a master regulator of development, had subtle effects on floral development. Our results indicate that small changes to MADS-box genes may have influenced the gradual evolution of floral form. This dissection of the effects of a single base-pair change, using an allelic series provided by evolution, is critical in this era of genome editing.

Next steps. Next projects are focused on explore mechanisms by which protein modifications and interactions affect floral organ formation and evolution. In the future, our findings might help to identify additional factors influencing floral development and evolution.

complexes may generate floral diversity by regulating different suites of downstream genes, thus contributing to evolutionary variation in organ shape and form (Mondragón-Palomino and Theissen, 2008; Theissen et al., 2016). For example, complexes of B- and E-class proteins may specify petal development in orchids (Orchidaceae species). However, the precise mix of B- and E-class proteins in these complexes likely differs between unelaborated petals and the highly elaborated petals that characterize orchid flowers (Hsu et al., 2015). Evolutionary changes to MADS box complexes, specifically to BCE MADS box complexes, may also have been important in the evolution of the flower itself (Wang et al., 2010; Theissen et al., 2016; Ruelens et al., 2017). Thus, combinatorial assembly of MADS box complexes may have been important in floral evolution and diversification.

Although differential MADS box complex assembly presents an appealing model for explaining floral diversification (Theissen and Saedler, 2001; Mondragón-Palomino and Theissen, 2009, 2011; Theissen et al., 2016; Bartlett, 2017), the consequences of changing MADS box protein-protein interactions have not been extensively tested in planta. If combinatorial MADS box complex assembly contributes to floral diversification, then we can predict (1) deep conservation of MADS box complexes like the BCE complex and (2) that evolutionary changes to floral MADS box protein-protein interactions should result in changes to gene regulation and, in turn, to floral development. Here, we test these predictions using the maize (*Zea mays*) B-class MADS box protein STERILE TASSEL SILKY EAR1 (STS1; a homolog of PISTILLATA in Arabidopsis; Goto and Meyerowitz, 1994; Bartlett et al., 2015). STS1 forms obligate heterodimers with SILKY1 (SI1; a homolog of APETALA3 in Arabidopsis; Jack et al., 1992; Ambrose et al., 2000; Whipple et al., 2004). We engineered an ancestral variant of STS1 that forms both homodimers and heterodimers with SI1 (Bartlett et al., 2016). We show that this facultative STS1 homodimerization has subtle, quantitative effects on stamen development but large effects on downstream gene expression. We also show that BCE complexes do form in maize. Lastly, we found that B-class dimerization affected MADS box complex composition and abundance. Our results show how coding change in a pleiotropic master regulator could have quantitative effects on MADS box complex composition and abundance and, in turn, contribute to quantitative variation in floral form.

RESULTS

STS1-HET and STS1-HOM Show Subtle Differences in Localization and Function

To explore the effects of B-class heterodimerization versus homodimerization, we developed transgenic maize plants that express a version of STS1 that can bind DNA as homodimers. We found that changing the Gly (G) residue at position 81 to Asp (D) reverts STS1 to its most likely ancestral dimerization state: able to form both homodimers and heterodimers with SI1 (Bartlett et al., 2016). Additional amino acid residues differ between STS1 and its most likely ancestor. However, we chose to introduce a single change (G81D) to explicitly test the effects of heterodimerization versus homodimerization, to the exclusion of other differences between the extant and ancestral proteins. We introduced the critical G81D change into an STS1-yellow fluorescent protein (YFP) fusion construct that rescues *sts1* (Bartlett et al., 2015) and used it to transform maize. We will refer to the obligate heterodimer construct (*pSTS1:STS1-YFP*) as *STS1-HET* and to the STS1 homodimer construct [*pSTS1:STS1(G81D)-YFP*] as *STS1-HOM*.

To understand how variable B-class dimerization affects floral development, we used identical crossing schemes to generate

lines carrying either *STS1-HET* or *STS1-HOM* in backgrounds that were segregating either *si1* or *sts1*. In both *si1* and *sts1*, stamen and lodicule (petal homolog) organ identity is lost (Ambrose et al., 2000; Bartlett et al., 2015). We found that both transgenes complemented *sts1*; neither organ identity nor organ number varied between *STS1-HET* and *STS1-HOM* (Figures 1D and 1E; Supplemental Table 1). In contrast, adult flowers in *si1* mutants carrying *STS1-HOM* were indistinguishable from nontransgenic *si1* mutants (Figures 1C and 1F). This indicates that *STS1-HOM* can rescue *sts1* mutants and is functional, but it cannot compensate for the loss of *SI1* function.

To explore differences between STS1-HET and STS1-HOM in more detail, we analyzed the development of complemented *sts1* mutants. We examined protein localization of both STS1-HET and STS1-HOM over the course of development using confocal microscopy. We found that STS1-HET was restricted to lodicule and stamen primordia, as expected (Figures 1G and 1H; Bartlett et al., 2015). In contrast, protein localization was relaxed in STS1-HOM lines, appearing in gynoecia in addition to lodicule and stamen primordia (Figure 1J). However, this gynoecial localization was not evident in our immunolocalizations using an anti-STS1 antibody (Supplemental Figure 1). In contrast to the proteins, *STS1-HET* and *STS1-HOM* RNAs showed similar localization patterns (Supplemental Figure 1). This suggests that the subtle localization differences we detected were regulated at the protein level.

In addition to protein localization differences, morphology differed quantitatively between *STS1-HOM* and *STS1-HET* flowers. This included differences in anther aspect ratio, such that anthers of *STS1-HOM* flowers were wider and shorter than those of *STS1-HET* flowers while they were still developing (Student's *t* test, P = 6.8e-10; Figures 1K and 1L; Supplemental Data Set 1). We assayed anther shape at anthesis using eFourier analysis, as implemented in the R package MOMOCS (Bonhomme et al., 2014). This analysis identified a small but significant difference in shape between anthers from *sts1* mutants complemented with either *STS1-HET* or *STS1-HOM* (MANOVA, P = 0.006). Anthers from *STS1-HET* flowers occupied a larger morphospace and tended to be wider than *STS1-HOM* anthers (Supplemental Figure 2). Indeed,

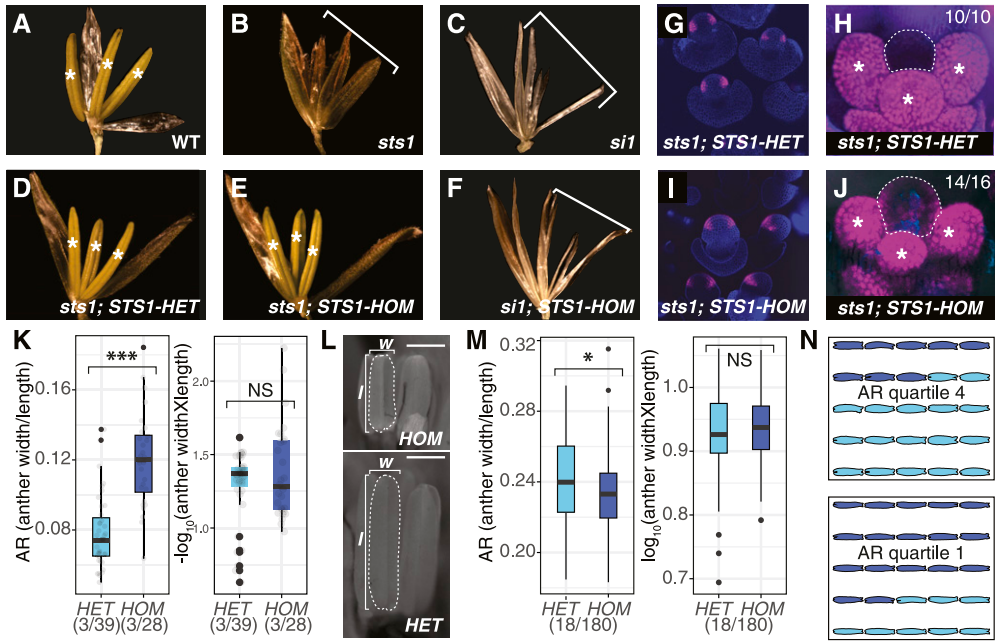

Figure 1. B-Class Dimerization Has Subtle Effects on Floral Development in Maize.

(A) to **(E)** Stamen identity (**[A]**; marked with asterisks) is lost in both *sts1* **(B)** and *si1* **(C)** mutant flowers. At anthesis, *sts1* mutant flowers complemented with either the *STS1-HET* **(D)** or *STS1-HOM* **(E)** transgene resemble wild-type flowers and each other.

(F) The *STS1-HOM* transgene did not complement the *si1* mutant phenotype.

(G) to **(J)** Confocal microscopy showing localization of STS1-HET (**[G]** and **[H]**) and STS1-HOM (**[I]** and **[J]**) localization in developing flowers. Dotted lines in **(H)** and **(J)** indicate developing gynoecia, and numbers in top right corners indicate frequencies at which we observed the shown localization patterns.

(K) to **(N)** Anther shape metrics during development (**[K]** and **[L]**) and at anthesis (**[M]** and **[N]**).

(K) During development, anther aspect ratio (AR; anther width/anther length) was higher in *STS1-HOM* anthers than in *STS1-HET* anthers (P = 6.8e-10; left), while anther area (anther width × anther length) was not significantly different (P = 0.2592; right). We measured 39 (*STS1-HET*) or 28 (*STS1-HOM*) anthers total from three individuals of each genotype. ***Highly Significant (P < 0.01); NS, not significant.

(L) Confocal images of developing anthers measured in **(K)**.

(M) At anthesis, anther aspect ratio is lower in *STS1-HOM* anthers than in *STS1-HET* anthers (P = 0.003; left), while anther area is not significantly different (P = 0.367; right). P values were calculated using Student's *t* tes. *Significant (P < 0.01); NS, not significant.

(N) Twenty-five randomly selected anthers from the first (bottom) and fourth (top) quartiles of anthers measured in **(M)**, colored according to STS1 transgene genotype. We measured 10 anthers from 18 individuals of each genotype (180 anthers per genotype).

aspect ratio measurements of mature anthers showed that anthers from *STS1-HOM* flowers were narrower than those from *STS1-HET* flowers (Student's *t* test, P = 0.003; Figures 1M and 1N; Supplemental Data Set 2). Differences in anther aspect ratio, both during development and at anthesis, were despite similarities in anther surface area, which we used as a proxy for size (developing anthers: Student's *t* test, P = 0.259 [Figure 1K]; anthesis: Student's *t* test, P = 0.367 [Figure 1M]). Taken together, our results suggest that B-class dimerization may affect anther shape, potentially by affecting anther growth dynamics over the course of development.

Differential Dimerization of Maize B-Class Proteins Affects Downstream Gene Regulation

The morphological differences between *STS1-HET* and *STS1-HOM* flowers were subtle, indicating small phenotypic consequences of differential B-class dimerization. We were curious if downstream transcription was similarly conserved between *STS1-HET* and *STS1-HOM*. To understand the effect of STS1 dimerization on gene expression, we performed RNA sequencing (RNA-seq) in *sts1* or *si1* mutants complemented with either *STS1-HET* or *STS1-HOM*. We harvested inflorescence tissue shortly after stamen primordium emergence to capture gene expression just after the initiation of *STS1* expression (Bartlett et al., 2015). Because of the high genetic diversity in maize, we compared expression profiles within genetic backgrounds to control for potential differences due to incomplete introgression of the *STS1* transgenes (Buckler et al., 2006). To this end, we measured differential expression by comparing expression in each line (*STS1-HOM* or *STS1-HET*) against expression in their mutant siblings.

These analyses revealed more differentially expressed genes in *STS1-HOM* than in *STS1-HET*, as compared with mutant siblings. At a 5% false discovery rate (FDR), there were 501 differentially expressed genes in inflorescences expressing *STS1-HET*, as compared with *sts1* mutant siblings (Figure 2A; Supplemental Data Set 3). In inflorescences expressing *STS1-HOM*, we found 1257 differentially expressed genes, as compared with *sts1* mutant siblings (Figure 2B; Supplemental Data Set 4). There were 109 genes differentially regulated by both *STS1-HOM* and *STS1-HET*. STS1-HOM can both homodimerize and heterodimerize with SI1 (Bartlett et al., 2016). To see how gene expression was affected specifically by STS1-HOM without the presence of SI1, we compared gene expression between inflorescences expressing either *STS1-HET* or *STS1-HOM* in a *si1* mutant background. We found that only 5 genes were differentially expressed in *STS1-HET* inflorescences, as compared with *si1* mutant siblings (Figure 2C; Supplemental Data Set 5). In contrast, in inflorescences expressing *STS1-HOM*, 91 genes were differentially expressed, as compared with *si1* mutant siblings (Figure 2D; Supplemental Data Set 6). These contrasts indicate that B-class dimerization affects patterns of gene expression in developing inflorescences, either directly or indirectly. Therefore, evolutionary change in B-class dimerization can impact downstream gene expression.

To determine whether the general functions of genes regulated by STS1-HET and STS1-HOM were qualitatively similar, we performed Gene Ontology (GO) enrichment analyses with our differentially expressed gene sets in an *sts1* mutant background (Supplemental Data Sets 7 and 8). To compare these lists of enriched GO terms, we used GO correlation plots (Figure 2E; Bergey et al., 2018). Since the *STS1-HET* and *STS1-HOM* constructs were so similar, and since our morphological data suggested subtle functional differences between *STS1-HET* and *STS1-HOM* (Figure 1), we reasoned that *STS1-HET* and *STS1-HOM* were regulating similar processes. Therefore, we made the threshold for calling a GO term unique to either data set very stringent; only GO terms with an enrichment $P < 0.01$ in one data set and an enrichment $P > 0.25$ in the other data set were called unique (Figure 2E, sectors i and v). Using these comparisons, we found many GO terms related to development shared between *STS1-HET* and *STS1-HOM* (Figure 2E). Indeed, 29 of the 65 enriched GO terms shared between *STS1-HET* and *STS1-HOM* were related to development ($P < 0.01$ in both data sets; Figure 1E, sector iii). GO terms related to signaling and metabolism were also enriched in both data sets, although more of these terms were specifically enriched in *STS1-HOM*. However, the most highly enriched GO terms in *STS1-HOM* were not significantly enriched in *STS1-HET* ($P > 0.25$). These GO terms, specific to *STS1-HOM*, were almost all related to chromatin assembly and protein modification (Figure 2E, sector i). Thus, core floral developmental programs were activated in inflorescences expressing *STS1-HOM*, but B-class dimerization also affected the expression of unique sets of genes, particularly genes involved in chromatin assembly and remodeling.

A Complex of B-, C-, and E-Class Proteins Is Conserved in Maize

Differential dimerization may affect the composition of protein complexes, which is crucial for MADS box function (Theissen and Saedler, 2001; Theissen et al., 2016). To determine how differential B-class dimerization might impact the composition of MADS box complexes, we performed immunoprecipitations (IPs) of STS1-HET and STS1-HOM in an *sts1* mutant background using a specific antibody against GFP (ChromoTek). We analyzed precipitated complexes using quantitative mass spectrometry (MS). After confirming the presence of STS1 in the IP complex through immunoblotting, we performed trypsin digestion and liquid chromatography-MS/MS followed by label-free protein quantification (Sinitcyn et al., 2018). We used protein from *sts1* mutant siblings as a negative control to detect nonspecific proteins. We compared abundances of identified proteins using the intensity-based absolute quantification (IBAQ) method (Krey et al., 2014; He et al., 2019). Protein identification was based on at least five exclusive peptides, and two replicates were performed for each sample; protein abundances were similar between replicates (Supplemental Data Sets 9 and 10). We found 1278 total proteins in complex with STS1-HET; 453 of these were either specific to STS1-HET or were at least twofold higher than in mutant siblings (Supplemental Data Set 9). In contrast, we found 1597 proteins in complex with STS1-HOM; 486 of these proteins were either specific to STS1-HOM or were at least twofold higher than in mutant siblings (Supplemental Data Set 10). We found 125 proteins in common to both the STS1-HET and STS1-HOM IPs (either absent in *sts1* siblings or twofold or greater change). This result indicates that, while many proteins are common to STS1-HET and STS1-HOM complexes, each STS1 variant is associated with a distinct set of proteins.

The first set of proteins in our IPs that we explored further were the MADS box proteins. Ancestral protein resurrection and in vitro surveys of protein-protein interactions predict that complexes of B-, C-, and E-class MADS box proteins are conserved across flowering plants (Veron et al., 2007; Theissen et al., 2016; Zhang et al., 2018). However, this prediction remains largely untested in planta, particularly in monocots. Therefore, we specifically searched for other MADS box proteins in our IP-MS data. In the STS1-HET IP-MS results, we found both STS1 and SI1 peptides as well as peptides for three E-class MADS box proteins (ZMM27, ZMM7, and ZMM6) and two C-class proteins (AGAMOUS co-orthologs ZAG1 and ZMM23; Supplemental Table 2; Münster et al. , 2002; Zahn et al., 2005). ZMM6, ZMM7, and ZMM27 are all in a single clade of E-class proteins, co-orthologous to the Arabidopsis protein SEPALLATA3 (Zahn et al., 2005). In STS1-HOM, we found the same three E-class proteins and one C-class protein, ZAG1, but did not find ZMM23. ZMM23 was identified as one of the most enriched proteins in the STS1-HET IP and was the only MADS box protein specific to STS1-HET. This variability in complex abundance between STS1-HET and STS1-HOM indicates that differential dimerization affects the mix of precisely which BCE complexes are present during floral development. Our results also indicate broad conservation of B-, C-, and E-class protein complexes between maize and Arabidopsis, confirming predictions from in vitro assays (Veron et al., 2007; Ruelens et al., 2017).

B-Class Dimerization Affects Transcription Factor Complex Abundance

The MADS box proteins we identified in both IP data sets were at much higher levels in STS1-HOM than in STS1-HET (SI1 was the only exception). STS1-HOM was far more abundant than STS1-HET: IBAQ values for STS1-HOM were 4.0 times higher than for STS1-HET, 3.58 times higher normalized to SI1 (Figure 3). The higher abundance of STS1-HOM in our IPs could have been due to complex stoichiometry, where STS1-HOM homodimerization caused double the number of STS1-HOM proteins in MADS box complexes. Alternatively, STS1-HOM protein levels could also have been generally higher in developing flowers. We suspected that STS1-HOM levels were generally higher; our immunolocalizations suggested a higher abundance of STS1-HOM versus STS1-HET, despite the same experimental conditions (Supplemental Figure 1). However, these immunolocalizations were not quantitative. To directly measure protein levels, we performed immunoblotting using a polyclonal antibody against STS1. The same amount of protein for each sample was loaded. After immunoblotting (described in Methods), we performed densitometry analysis using ImageJ (1.4 NIH software; Schneider et al., 2012). Relative abundance was calculated by dividing the densitometry value of STS1 protein with the respective loading control (α-Tubulin). In these blots, STS1-HOM was seven times more abundant than STS1-HET (Figure 3C; Supplemental Table 3). Together with our IP-MS results, these data indicate that STS1-HOM accumulated to a higher abundance than STS1-HET in inflorescence tissue.

STS1-HOM protein could have been more abundant than STS1-HET protein because the *STS1-HOM* transgene was transcribed to higher levels than the *STS1-HET* transgene. To test for this, we performed RT-qPCR using specific primers for *STS1* and *SI1* in *sts1* mutants complemented with either *STS1-HET* or *STS1-HOM*. We found that *SI1* was expressed to the same level in both lines; however, the expression of *STS1* in *STS1-HET* was 3.7-fold higher than in *STS1-HOM* (relative to *Actin*; Figure 3D). Similarly, in our RNA-seq results, normalized *STS1-HET* expression was consistently double normalized *STS1-HOM* expression: ~15,000 counts versus 8600 counts, respectively. Thus, despite relatively low *STS1-HOM* expression, STS1-HOM protein accumulated to higher levels than STS1-HET in floral tissue. This indicates that STS1 homodimerization led to increased protein accumulation independent of RNA levels. Therefore, the higher abundance of STS1-HOM is likely regulated posttranscriptionally.

The other MADS box proteins we detected in our IPs were also more abundant in STS1-HOM than in STS1-HET. ZAG1, ZMM6, and ZMM7 increased in abundance twofold to ninefold in STS1-HOM as compared with STS1-HET (Figure 3B; Supplemental Table 2). This higher abundance of ZAG1, ZMM6, ZMM7, and ZMM27 could also have been because of differences in transcription or differences posttranscriptionally. To distinguish between these possibilities, we looked for these genes in our RNA-seq data and determined that they were not differentially expressed between *STS1-HOM* and their *sts1* mutant siblings (Supplemental Data Set 4). Therefore, the higher abundance of these C- and E-class MADS box proteins was likely not because of higher transcription. Of all the MADS box proteins we identified in our IPs, SI1 was the only one found at similar levels in both STS1-HET and STS1-HOM. This suggests that SI1 is able to compete with STS1-HOM to form heterodimers and that SI1 may be a limiting factor in MADS box protein complex assembly. Taken together, our results show that STS1 homodimerization affected the abundance of other MADS box proteins in transcription factor complexes, likely posttranscriptionally.

STS1-HET and STS1-HOM Form Complexes With Chromatin Remodelers, Kinases, and the Ubiquitination Machinery

To explore our IP-MS data sets further, we performed GO enrichment analyses with identified proteins in the STS1-HET versus STS1-HOM IPs. In these analyses, we only included proteins with at least a twofold change as compared with *sts1* siblings. When we compared the resulting lists of enriched GO terms, our results were similar to the RNA-seq comparisons: development, signaling, and metabolism-related GO terms were enriched in both data sets. However, chromatin-related GO terms were no longer exclusively enriched in the STS1-HOM data set (Figures 2E and 3A; Supplemental Data Sets 11 and 12).

We found GO categories related to chromatin modification enriched in both the STS1-HOM and STS1-HET IP-MS results (Figure 3A). Many of the proteins that were in these enriched GO categories are homologs of Arabidopsis chromatin remodelers that act to relieve the chromatin-mediated repression of transcription (Wu et al., 2012; Hu et al., 2014; Li et al., 2015). This includes an ISWI chromatin-remodeling complex ATPase, CHR126b, a homolog of the Arabidopsis protein CHR11 (Smaczniak et al., 2012). CHR126b was enriched in both the STS1-HET and STS1-HOM IP-MS data

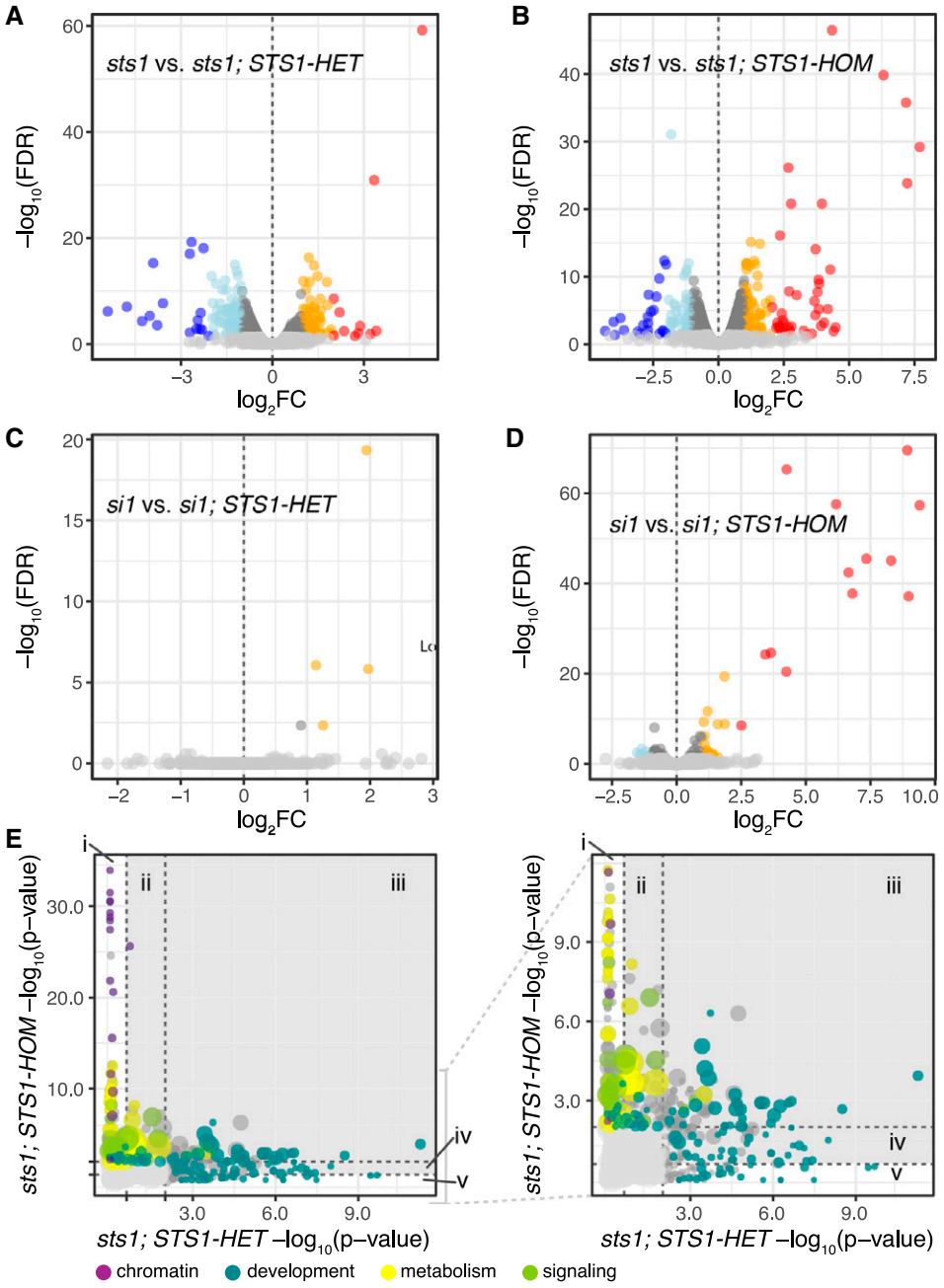

Figure 2. B-Class Dimerization Remodels Transcription in Developing Tassel Flowers.

(A) to **(D)** Significantly more genes are differentially expressed in *STS1-HOM* versus *STS1-HET* inflorescences, as compared with mutant siblings.
(A) and **(B)** Differential gene expression in *sts1* mutants complemented with either the *STS1-HET* **(A)** or *STS1-HOM* **(B)** transgene, as compared with *sts1* mutant siblings.
(C) and **(D)** Differential gene expression in *si1* mutants complemented with either the *STS1-HET* **(C)** or *STS1-HOM* **(D)** transgene, as compared with *si1* mutant siblings.
(E) GO term correlation plots comparing probabilities of GO term enrichments in *STS1-HET* versus *STS1-HOM*. GO categories related to chromatin assembly and remodeling are significantly enriched in the *STS1-HOM* DE gene set. The left panel shows all GO terms, and the right panel excludes highly enriched GO terms in *STS1-HOM*. Dot sizes are proportional to the number of genes in each enriched GO term category and colored according to which larger category they are associated with. P value cutoffs for sectors are as follows: (i) P value x > 0.25 and P value y < 0.01; (ii) 0.01 < P value x < 0.25 and P value y < 0.01; (iii) P value x < 0.01 and P value y < 0.01; (iv) P value x < 0.01 and 0.01 < P value y < 0.25; (v) P value x < 0.01 and P value x > 0.25.

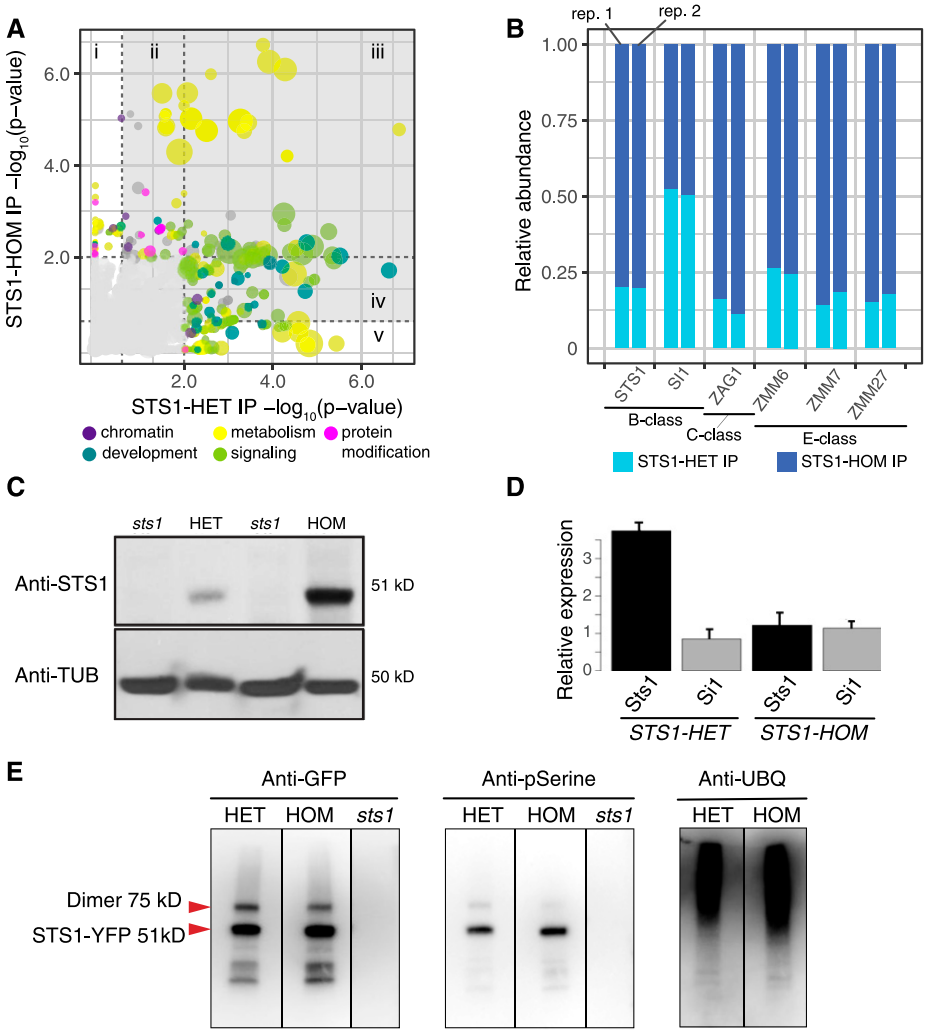

Figure 3. B-Class Dimerization Affects Protein Abundance and Protein Complex Assembly in Developing Tassels.

(A)GO term correlation plot comparing probabilities of GO term enrichments in the STS1-HET versus STS1-HOM IP-MS data sets. GO categories related to protein modification and chromatin remodeling are enriched in both data sets. Dot sizes are proportional to the number of genes in each enriched GO term category and colored according to which larger category they are associated with. P value cutoffs for sectors are as follows: (i) P value x > 0.25 and P value y < 0.01; (ii) 0.01 < P value x < 0.25 and P value y < 0.01; (iii) P value x < 0.01 and P value y < 0.01; (iv) P value x < 0.01 and 0.01 < P value y < 0.25; (v) P value x < 0.01 and P value x > 0.25.

(B) Relative abundances of MADS box proteins in the IP-MS data sets. STS1, as well as C- and E-class proteins, are higher in STS1-HOM than in STS1-HET IPs.

(C) Immunoblots with anti-STS1 (top) and anti-Tubulin (bottom) also show that STS1-HET is less abundant than STS1-HOM.

(D) RT-qPCR shows that *STS1-HET* RNA is more abundant than *STS1-HOM* RNA, relative to *Actin*. *SI1* RNA occurs at similar levels, relative to *Actin*, in both *STS1-HET* and *STS1-HOM*.

(E) Immunoblots with anti-pSer and anti-ubiquitin show that STS1-HET and STS1-HOM are phosphorylated and likely in complex with ubiquitinated proteins. The same amount of immunoprecipitated STS1-HET and STS1-HOM protein was loaded for this experiment.

sets (Supplemental Table 2). We found three additional chromatin remodeling and scaffolding factors in complex only with STS1-HOM: BRAHMA1, CHR12, and FRIGIDA-LIKE PROTEIN4a (Supplemental Table 2). In Arabidopsis, BRAHMA, CHR12, and FRIGIDA modify specific chromatin states to regulate the transition to floral meristem identity, floral organ development, and meristem determinacy (Bezhani et al., 2007; Liu et al., 2009; Sang et al., 2012; Wu et al., 2012; Hu et al., 2014; Thouly et al., 2020). In complex with STS1-HOM, these proteins might be acting to open up chromatin surrounding MADS box binding sites, resulting in higher or more prolonged expression of MADS box targets in *STS1-HOM* plants (Figure 4).

We also found a class of proteins related to signaling in our IP data sets, specifically kinases. Ten kinases were immunoprecipitated with STS1-HET and 11 with STS1-HOM; only two of these were in both samples (Supplemental Data Sets 9 and 10; Supplemental

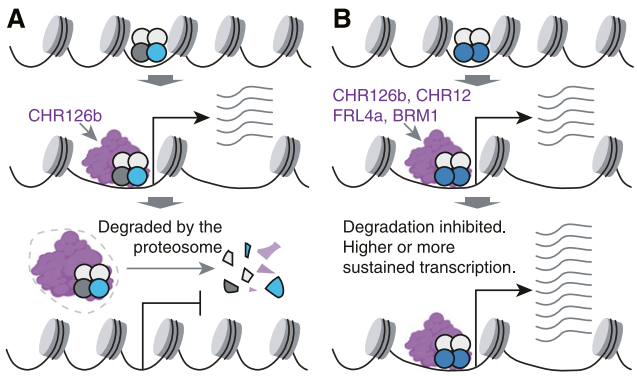

Figure 4. An Activation-Degradation Model for the Consequences of Differential B-Class Dimerization.

(A) STS1-HET/SI1 heterodimers, in complex with other MADS box proteins, recruit chromatin remodelers like the SWI/SNF ATPase CHR126b, ultimately resulting in the upregulation of target genes. This transcription is likely halted by the proteasome-mediated degradation of MADS box complexes.

(B) STS1-HOM homodimers and their MADS box partners also recruit chromatin remodelers and scaffolding proteins, resulting in upregulated transcription. However, STS1 homodimerization disrupts degradation, resulting in higher or more sustained transcription of target genes. BRM1, BRAHMA1; FRL4a, FRIGIDA-LIKE PROTEIN4a.

Table 4). The kinases found in both STS1-HET and STS1-HOM were a nonspecific Ser/Thr protein kinase (Zm00001d028733) and Calcium-dependent protein kinase11 (Zm00001d004812). In Arabidopsis, calcium-dependent protein kinases are involved in signal transduction pathways that involve calcium as a second messenger and regulate the calcium-mediated abscisic acid signaling pathway (Zhu et al., 2007). In general, the kinases found only with STS1-HET were related to basal metabolism, for example a phosphoglycerate kinase and a pyruvate kinase, likely involved in the synthesis and degradation of carbohydrates (Lu and Hunter, 2018; Rosa-Téllez et al., 2018). In contrast, the kinases that immunoprecipitated with STS1-HOM were related to signaling and membrane receptors, for example brassinosteroid (BR)-signaling kinase2 and BR-LRR receptor kinase (Tang et al., 2008; Xu et al., 2014). No kinases have been reported as MADS interactors in Arabidopsis (or any other taxon); this might have been because of IP conditions (Smaczniak et al., 2012). Further analyses are necessary to confirm interactions between STS1 and the kinases we found.

One new set of GO terms that emerged in our analysis was related to protein modification and ubiquitination. These GO terms were more enriched in STS1-HOM but were still present in STS1-HET (Figure 3A). When we explored which proteins might be represented by these enriched GO terms (Supplemental Table 5), we found five proteins from the Cul4-RING E3 ubiquitin ligase complex (homologous to the Arabidopsis proteins CAND1, CUL1, CUL4, XPO1A, and DCD) in the STS1-HOM IP, two of which (CAND1 and CUL1 homologs) were also in the STS1-HET IP-MS data set (Feng et al., 2004; Chen et al., 2006; Adhvaryu et al., 2015). We also found three proteins from the Anaphase-Promoting Complex or Cyclosome (APC/C) only in the STS1-HOM data set; the APC/C is another E3 ubiquitin ligase complex (Wang et al., 2012, 2013; Xu et al., 2019). Although neither the Cul4-RING E3 ubiquitin ligase complex nor the APC/C have been reported as interacting with MADS box proteins, the E3 ubiquitin ligase proteins we found in our IPs are in the same complexes in other species, giving us additional confidence in our results (Feng et al., 2004; Wertz et al., 2004; Adhvaryu et al., 2015; Chang et al., 2015). Thus, our IP-MS results indicate that MADS box complexes in maize interact with the ubiquitination machinery.

STS1-HET and STS1-HOM Are Posttranslationally Modified

STS1-HOM was more abundant than STS1-HET, and both proteins were in complex with ubiquitination machinery and kinases in our IP-MS results (Figure 3). Ubiquitination and (often) phosphorylation precede protein degradation in the proteasome (Schrader et al., 2009). Therefore, our IP-MS data suggested that STS1 degradation was regulated by posttranslational modification. To explore the posttranslational modification of STS1, we first predicted phosphorylation sites in STS1-HET and STS1-HOM using Musite (Gao et al., 2010; Yao et al., 2012). The results for STS1-HET and STS1-HOM were identical and revealed a high likelihood for STS1 phosphorylation, mostly in Ser residues in the I and K domains, which mediate protein-protein interactions (Masiero et al., 2002; Yang et al., 2003; Bartlett et al., 2015). Similarly, in silico analyses using UbPred revealed low-confidence ubiquitination sites in both STS1-HET and STS1-HOM (Radivojac et al., 2010). These analyses led us to explore the phosphorylation and ubiquitination of STS1-HET versus STS1-HOM in vitro. To do this, after IP of STS1-containing complexes using an anti-GFP antibody (Roche), we performed immunoblotting using commercial anti-pSer or anti-ubiquitin monoclonal antibodies (Santa Cruz Biotechnology). We found that both STS1-HET and STS1-HOM proteins were phosphorylated. When we analyzed IP complexes with an anti-ubiquitin antibody, we identified potentially ubiquitinated proteins in both the STS1-HET and STS1-HOM complexes. We detected no obvious differences in phosphorylation or ubiquitination between STS1-HET and STS1-HOM (Figure 3E). However, these blots were not quantitative and would not have revealed subtle differences between STS1-HET and STS1-HOM posttranslational modifications. Our results do indicate that STS1-HET and STS1-HOM are potentially in complex with ubiquitinated proteins and are both phosphorylated.

DISCUSSION

We found that differential B-class dimerization did not result in qualitatively different organ identities in maize. Instead, the impacts of differential B-class dimerization on maize floral development were subtle and quantitative: anthers from *STS1-HOM* flowers were narrower than those from *STS1-HET* flowers at anthesis (Figure 1). At a molecular level, we found STS1 in complex with C- and E-class proteins, chromatin remodelers, and chromatin scaffolding proteins. In Arabidopsis, MADS box proteins also associate with chromatin remodelers and scaffolding proteins (Smaczniak et al., 2012; Vachon et al., 2018). Thus, both BCE MADS box complexes and MADS box interaction with chromatin proteins are conserved between maize and Arabidopsis. We found that STS1-HOM was more abundant than STS1-HET and that the two STS1 variants were in complex with different mixes of

MADS box proteins and chromatin remodelers. In Arabidopsis, the differential abundance and composition of transcription factor complexes, as well as the differential recruitment of chromatin remodeling factors, can all impact the dynamics of transcription (Li et al., 2015; Hugouvieux et al., 2018; Clark et al., 2020). Indeed, we found that B-class dimerization had profound effects on gene expression (Figure 2). Importantly, while the DNA binding profiles of STS1-HET and STS1-HOM dimers may differ, this difference is not essential for altered transcriptional dynamics. Differential MADS box complex abundance and differential recruitment of chromatin-modifying machinery, mediated by protein-protein interactions, may result in quantitative tuning of transcription (Figure 4).

We found that STS1-HOM protein was more abundant than STS1-HET, despite lower levels of RNA (Figure 3). This means that STS1-HOM abundance was likely regulated posttranscriptionally, leaving either (1) impaired degradation of the STS1-HOM protein or (2) increased translational efficiency of the *STS1-HOM* transcript as explanations for higher STS1-HOM abundance (Schrader et al., 2009; Gingold and Pilpel, 2011). We favor impaired degradation of STS1-HOM for three reasons. First, the *STS1-HET* and *STS1-HOM* transcripts differ by a single nucleotide in the 81st codon (Bartlett et al., 2016). Although this single-nucleotide polymorphism could affect RNA secondary structure and translation efficiency, it is well downstream of the start codon, where RNA secondary structure is more likely to affect translational efficiency (Kudla et al., 2009; Tzeng et al., 2009; Tuller et al., 2010; Ding et al., 2014; Verma et al., 2019). Second, both STS1 variants coprecipitated with proteins related to ubiquitination. Third, STS1 includes a KEN box sequence, unaffected by the G81D change that differentiates STS1-HET from STS1-HOM. KEN boxes are short linear motifs (degrons) recognized by the APC/C, an E3 ubiquitin ligase (Davey and Morgan, 2016). This indicates that STS1 may be recruiting the APC/C. Indeed, we found three APC/C subunits in complex with STS1-HOM. The higher abundance of STS1-HOM may have allowed us to detect these transient interactions. Beyond our own data, many Arabidopsis MADS box proteins are ubiquitinated (Manzano et al., 2008), and some MADS box complexes are sent to the proteasome for degradation under phytoplasma infection (MacLean et al., 2014). Taken together, these data lead us to favor differential protein degradation as an explanation for higher STS1-HOM abundance.

It seems likely that STS1-HOM was more abundant than STS1-HET because of differential degradation. However, we are left wondering what mechanism may underlie this difference. Both differential dimerization and DNA binding affinity can affect protein degradation in the proteasome (Johnson et al., 1998; Coppotelli et al., 2011; Kiparaki et al., 2015; Hickey et al., 2018); either may be responsible for differential degradation of STS1-HET versus STS1-HOM. For example, the yeast (*Saccharomyces cerevisiae*) homeodomain transcription factor MATα2 both homodimerizes and forms heterodimers with a paralog, MATa1. While the MATα2 homodimers are ubiquitinated and rapidly degraded, a degron in MATα2 is masked by heterodimerization with MATa1 (Johnson et al., 1998). In the case of STS1, the KEN box degron, or an as-yet unidentified degron (Moss et al., 2015; Geffen et al., 2016; Ella et al., 2019), may be masked or altered in STS1 homodimers but not in STS1/SI1 heterodimers, allowing for more rapid degradation of STS1-HET. The strength of DNA binding by a protein can also affect degradation dynamics (Coppotelli et al., 2011; Hickey et al., 2018). In yeast, MATα2 mutant proteins that differ in their DNA binding profiles are far more stable than wild-type proteins, despite intact degron sequences (Hickey et al., 2018). Similarly, strong DNA binding of an Epstein-Barr virus protein inhibits its degradation in the proteasome (Coppotelli et al., 2011). STS1 homodimers and STS1/SI1 heterodimers may differ in their DNA binding profiles or affinity, which could, in turn, affect protein degradation dynamics.

We discovered that STS1 likely interacts with kinases and is phosphorylated (Figure 3). Phosphorylation is an important posttranslational modification that impacts protein function by controlling subcellular localization, DNA binding, and protein-protein interactions (Wang et al., 2018; Xu et al., 2018; Millar et al., 2019). A potential Ser/Thr phosphorylation site within the MADS box domain is deeply conserved in plants, suggesting the importance of phosphorylation for MADS box protein function (Angenent and Immink, 2009; Patharkar and Walker, 2016). Indeed, several MADS box proteins are phosphorylated. For example, phosphorylation of the mouse MADS box protein MEF2C enhances its DNA binding activity (Molkentin et al., 1996). In Arabidopsis, AGL24 is bound and phosphorylated by a meristematic receptor-like kinase (Fujita et al., 2003). AGL15 is bound and phosphorylated by MPK3/6, allowing for the expression of *HAESA*, a Leu-rich repeat receptor-like kinase gene that regulates floral organ abscission (Patharkar and Walker, 2016). Although phosphorylation of ribosomes impacts the translational efficiency of B-class mRNAs (Tzeng et al., 2009), we could find no reports of B-class protein phosphorylation. Our demonstration of in planta phosphorylation of STS1 could contribute to understanding of the regulation of B-class MADS box proteins.

We found that variation in B-class MADS box dimerization affected one aspect of anther shape in maize: anthers from *STS1-HOM* flowers were narrower than those from *STS1-HET* flowers. This could be because of altered transcription of genes regulating cell division or expansion in *STS1-HET* versus *STS1-HOM* (Figure 4). Indeed, GO categories specifically enriched in the *STS1-HOM* DE gene set include "regulation of cell size," "cell proliferation," and "response to gibberellin" (Supplemental Data Set 8). Upregulated genes in these GO categories encode putative cell cycle regulators and markers of proliferating cells, including proliferating cell nuclear antigens and histones (Citterio et al., 1992; Fobert et al., 1994). Importantly, many of these genes are also in the chromatin categories that were highly enriched in the *STS1-HOM* DE gene set (Figure 2). We think that this enrichment indicates both altered regulation of cell division and altered chromatin remodeling caused by the higher abundance of STS1-HOM. Three *SHORT INTERNODE/STYLISH* (*SHI/STY*) transcription factor genes are specifically upregulated in *STS1-HOM*. SHI/STY transcription factors regulate organ morphogenesis and plant architecture in many taxa, including in the grasses barley (*Hordeum vulgare*) and rice (*Oryza sativa*; Kuusk et al., 2006; Yuo et al., 2012; Landberg et al., 2013; Gomariz-Fernández et al., 2017; Youssef et al., 2017; Duan et al., 2019; Min et al., 2019). In barley and Arabidopsis, *SHI/STY* genes have specific roles in positive regulation of cell proliferation (Kuusk et al., 2006; Yuo et al., 2012).

The upregulated *SHI/STY* genes may similarly be regulating cell proliferation in *STS1-HOM* anthers. Thus, differential B-class dimerization might impact the regulation of cell division in developing anthers, resulting in quantitative differences in anther shape.

Small changes to floral organ development, regulated by MADS box genes, are significant in the evolution of floral diversity. Within families and genera, large-scale changes to floral Bauplan are rare. Instead, changes to organ shape, size, color, and micromorphology are more common (Endress, 1992; Rudall and Bateman, 2004; Bartlett and Specht, 2010; Cui et al., 2010). These small differences in organ form can have important consequences for floral function. For example, in *Plantago* and *Thalictrum,* stamen dimensions and material properties are important for efficient pollen release from anthers (Timerman et al., 2014; Timerman and Barrett, 2019). In *Primula*, variation in anther height is critical in the evolution of heterostyly and is likely regulated by a B-class gene, a *PI* homolog (Li et al., 2016). Similarly, B-class MADS box genes regulate specific organ traits in a number of taxa, including petal and stamen size in Arabidopsis (Wuest et al., 2012), petaloidy in *Aquilegia* (Sharma and Kramer, 2017), and petal fusion in *Petunia* and *Nicotiana* (Vandenbussche et al., 2004; Geuten and Irish, 2010). Indeed, similar roles for B-class genes beyond early organ specification are likely widespread; B-class genes are expressed until late in floral development in many taxa (Kim et al., 2005; Kramer et al., 2007; Hileman and Irish, 2009; Bartlett et al., 2015). Critically, null mutant phenotypes can obscure roles for master regulators like the B-class genes in regulating individual organ traits. In contrast, our dissection of the consequences of evolutionary change in protein sequence revealed a specific function for a pleiotropic gene.

The small phenotypic change that we found indicates that floral development is largely robust to evolutionary shifts in B-class MADS box dimerization. This robustness may be important in the evolution of floral form. Developmental robustness may allow diversity in MADS box protein-protein interactions to accumulate (Zhang et al., 2018). This cryptic molecular diversity may contribute to the overall evolvability of floral morphology. When genetic variation can accumulate in a developmental system without seriously impacting organismal phenotype or fitness, this hidden genetic variation can allow for rapid change under future selective pressure (i.e., the system can become more "evolvable"; Wagner, 2012). At a morphological level, floral traits like the lengths of stamens, stigmas, and corolla tubes are evolvable and can change under selection after only short periods of time (Conner et al., 2011; Opedal et al., 2017; Opedal, 2019). Selection on floral form may also not be limited by genetic variation, indicating that there is genetic variation in the molecular networks that regulate flower development (Ashman and Majetic, 2006). Variation in MADS box protein-protein interaction networks may represent some of the molecular genetic variation that allows for floral evolvability, acting as grist for the mill of natural selection (Zhang et al., 2018).

In all of our experiments, we focused on a single maize PI-like protein, STS1. However, there are three PI co-orthologs in maize: STS1, ZMM18, and ZMM29 (Münster et al., 2002). Although neither *ZMM18* nor *ZMM29* can compensate for the loss of *STS1* function, both are very similar to STS1 at the protein level, both are expressed in developing flowers, and both form obligate heterodimers with SI1 (Bartlett et al., 2015). Together with the three C-class paralogs and three SEPALLATA3 co-orthologs in maize (Zahn et al., 2005), these extra B-class paralogs could add further diversity to the mix of BCE MADS box complexes present during floral development. These complexes may also differ in their DNA binding profiles, adding yet more complexity. This complexity, and the high potential for evolutionary variation in MADS box protein-protein interactions (Veron et al., 2007; Bartlett et al., 2016; Silva et al., 2016; Zhang et al., 2018), adds further capacity for transcriptional tuning and quantitative variation in the evolution of floral development. To dissect this complexity further, *Brachypodium distachyon* offers an ideal system to work with in conjunction with maize. *B. distachyon* has a single STS1 ortholog, capable of both homodimerization and heterodimerization with SI1, is a tractable genetic system, and has a smaller complement of MADS box proteins than maize (Münster et al., 2002; Opanowicz et al., 2008; Wei et al., 2014; Bartlett et al., 2016).

The transcriptional tuning mediated by differential B-class dimerization that we discovered has important consequences for the evolution of floral development. In the grasses and the broader Poales, where STS1-like homodimerization is common (Bartlett et al., 2016), the relative mix of B-class heterodimers versus homodimers may impact the abundance of MADS box complexes and the recruitment of chromatin remodeling factors, as in maize. This could affect downstream transcription and, in turn, the dynamics of development. Beyond the Poales, very few MADS box protein-protein interactions have been examined in a comparative framework. However, given (1) evolutionary variation in interactions between B-class proteins (the least promiscuous of the floral MADS box proteins), (2) the propensity for rapid evolution of MADS box protein-protein interactions, and (3) lineage-specific MADS box gene duplications, MADS box protein-protein interaction profiles are likely diverse within families and genera (Mondragón-Palomino and Theissen, 2009; Melzer et al., 2014; Bartlett et al., 2016; Silva et al., 2016; Alhindi et al., 2017). This diversity could be quantitatively altering transcriptional dynamics and floral development, as with STS1-HET versus STS1-HOM in maize. Thus, evolutionary variation in a pleiotropic master regulator like STS1 could impact transcriptional dynamics and have small, quantitative effects on floral development and the evolution of floral diversity.

METHODS

Transgenic Lines and Plant Growth

STS1 transgenes, in the pTF101 vector backbone, were transformed into the maize (*Zea mays*) Hi-II genetic background at the Iowa State University plant transformation facility (annotated vector maps are included in the data repository). *STS1-HET* and *STS1-HOM* transformants were crossed to either *sts1* or *si1* mutants in the A619 genetic background. Resulting progeny carrying a transgene were identified by their ability to resist herbicide application and crossed again to *sts1* or *si1* mutants in the A619 genetic background. Once generated, plants for all molecular analyses were grown in the University of Massachusetts College of Natural Science greenhouse using a 50:50 soil mix of LC1 (SunGro Horticulture) and Turface (Turface). Field-grown plants were grown at the University of Massachusetts Crop and Animal Research and Education Farm in South Deerfield, Massachusetts.

RNA-Seq Tissue Collection and Sequencing

Plants were grown in the greenhouse as described above. Shortly after stamen primordium emergence (4 to 5 weeks after planting), plants were harvested and inflorescence meristems were flash frozen in liquid nitrogen. Samples were harvested at the same time of day, beginning at 3 PM. Three plants per genotype were pooled to generate one biological replicate, with three biological replicates per genotype (genotyping primers are listed in Supplemental Table 6). RNA was extracted from each pooled biological replicate using a combination of Trizol (Invitrogen) and Qiagen Plant RNeasy columns including Qiagen on-column DNase digestion. One microgram of RNA from each biological replicate was used for RNA library preparation with the NEBNext Ultra library kit per the manufacturer's instructions (three libraries per genotype). Samples were barcoded using NEBNext Set 1 Multiplex Oligos for Illumina to generate libraries for single-end 150-bp sequencing. DNA sequencing was performed at the Genomics Resource Laboratory, University of Massachusetts at Amherst, using an Illumina NextSeq500.

Differential Expression Analysis

Quality and adapter filtering were performed as part of the Illumina pipeline. Reads were mapped to the version 4 maize genome assembly Zm-B73-REFERENCE-GRAMENE-4.0 using STAR v2.5.3a (Dobin et al., 2013; Jiao et al., 2017). Mapping using STAR included default parameters for alignment and seeding, quality filtering, trimming, and removal of alignments with noncanonical splice junctions to obtain counts per gene (Dobin et al., 2013). Differential expression analysis was performed using the R package RUVseq for normalization followed by differential expression analysis with edgeR (Robinson et al., 2010; McCarthy et al., 2012; Risso et al., 2014). The RUVseq pipeline included upper quartile normalization using 7000 empirically determined control genes. These empirical control genes are the 7000 least differentially expressed genes in the data set as determined by the analysis pipeline. Where samples did not separate clearly by our experimental variables (e.g., genetic background), those samples were not included in the downstream differential expression analysis, resulting in the exclusion of one STS1-HET and one STS1-HOM library.

GO Analysis

GO analysis was completed using the R package GOseq (Young et al., 2010), utilizing the maize-PANNZER GO annotations from maize-GAMER (Wimalanathan et al., 2018), using the default parameters. The RNA analysis included all genes from the *STS1-HET* and *STS1-HOM* RNA-seq analysis with FDR $\leq$ 0.05, and the proteomics analysis included the 100 genes with the highest fold change from the STS1-HET and STS1-HOM data sets. Genes without a GO annotation were excluded during the analysis.

Confocal Microscopy

Plants were grown in the greenhouse as described above. Shortly after stamen primordium emergence (4 to 5 weeks after planting), plants were harvested and meristems were stained with 5 μM SynaptoRed membrane dye (VWR 80510-682) in DMSO. The confocal image data were gathered using an A1R: Nikon A1 Resonant Scanning Confocal Microscope.

Anther Shape Measurement and Analysis

For measuring anthers and counting floral organs, we grew plants in the greenhouse (young anthers) or field (anthers at anthesis) as described above. To measure anthers in young flowers, plants were harvested at the inflorescence meristem stage after glume development (5 to 6 weeks after planting). Developing flowers were imaged using Leica CTR5500 fluorescence and Zeiss 710 confocal microscopes. Anthers were measured in three individuals per genotype, more than six anthers per individual. To measure anthers at anthesis, dehisced anthers were harvested from the central spike on the day that flowers first opened. Anthers with filaments attached were harvested from central spikes and scanned within 1 h after dehiscing. Individual anthers were placed on a slide (flat side down) and scanned using an Epson V700 scanner. Scanned images were separated into individual files, and images were made binary using ImageJ (Schneider et al., 2012). For the anther aspect ratio, individual anther image files were read into R, and anther length and width were measured using the R package MOMOCS (Bonhomme et al., 2014). Anther aspect ratio was calculated by dividing anther width by anther length (18 individuals per genotype, 10 anthers per individual). These aspect ratio values were log-transformed (log base 10) for normality (Shapiro-Wilk normality test, $P = 0.66$). Means of log-transformed aspect ratio values were compared using Student's *t* test (Supplemental Table 7). For the eFourier analysis, individual anther image files were read into R, and analysis was completed using the R package MOMOCS (Bonhomme et al., 2014). The eFourier transformation was done using 12 harmonics and normalization of coefficients. Statistical analysis was completed using MANOVA.

For the organ counts, mature anthers were harvested from the central spike prior to dehiscence, and we counted lodicules and stamens in five spikelets from five individuals (50 florets total). All anther measurements are given in Supplemental Data Sets 1 and 2, and anther images are included in the data repository.

IP

For each genotype (*STS1-HET*, *STS1-HOM,* and matched *sts1* mutant siblings), 5 g (40 plants) of pooled maize tassels (0.5 to 1.0 cm in length) was ground in liquid nitrogen using mortar and pestle. The resulting powder was mixed with 10 mL of an extraction buffer for proteins dynamically transported between nucleus and cytosol, in native conditions (50 mM Tris-HCl, pH 7.5, 150 mM NaCl, 1% [w/v] IGEPAL-CA-630, and 1× protease inhibitor mix). Then, extract was filtered through four layers of Miracloth and centrifuged twice at 15,000*g* for 10 min at 4°C. Protein extract was incubated with 40 μL of GFP-trap MA bead slurry (ChromoTek), shaking for 2 h at 4°C. Beads with the bound target protein were magnetically separated and washed four times with 200 μL of ice-cold wash buffer containing 50 mM Tris, pH 7.5, 150 mM NaCl, 0.1% (w/v) IGEPAL-CA-630, and 1× protease inhibitor mix. Bound proteins were eluted with 40 μL of elution buffer (0.05% [w/v] bromophenol blue, 0.1 M DTT, 10% glycerol [v/v], 2% SDS [w/v], and 0.05 M Tris-HCl, pH 6.8). Five microliters was used for immunoblotting to confirm the presence of the bait protein (STS1-YFP) by standard SDS-PAGE and detection by chemiluminescence with a monoclonal anti-GFP antibody (Mouse IgG1K, clones 7.1 and 13.1; Roche catalog no. 11814460001) at 1:1000 dilution and anti-mouse HRP-conjugated secondary antibody (Amersham ECL GE catalog no. 45,001,275) at 1:3000 dilution. Then, 35 μL was used to run a short SDS-PAGE gel, stained with GelCode Blue Safe protein stain (Thermo Fisher Scientific). Gel slices were sent for MS analysis to the University of Massachusetts Medical School MS facility. Two replicates were performed for each genotype.

Liquid Chromatography-MS/MS and Label-Free Protein Quantification

In-gel trypsin digestion was analyzed in a quadrupole-Orbitrap hybrid mass spectrometer (Thermo Sci Q-Exactive with Waters NanoAcquity UPLC). Forty individuals of each genotype (*sts1* and *sts1* mutants complemented with STS1-HET or STS1-HOM) were used for each IP experiment. When a high number of individuals is used, a lower number of technical replicates

in the mass spectrometer is needed to get robust results (Jorrín-Novo et al., 2015). In this experiment, the reproducibility can be observed in the high number of proteins identified in both replicates for each sample as well as in the similar abundance of each one (Supplemental Data Sets 9 and 10). For protein identification, Mascot in Proteome Discoverer 2.1.1.21 with the Uniprot_Maize database was used. For label-free quantification, Scaffold version 4.8.4 was used, with 90% minimum peptide threshold, three peptides minimum, and a peptide FDR of 0.05.

Antibody Production and Immunolocalization

Anti-STS1 antibody was developed from the full-length coding sequence of *STS1* cloned into pDEST17 at the Bartlett lab, using the protocol described by Chuck et al. (2014) with some modifications. 6HIS-STS1 was expressed and purified from *Escherichia coli* Rosetta strain, using denaturing conditions. A total of 200 μg of purified protein was sent to Cocalico Biologicals, where two guinea pig immunizations were performed. Serum was used for antibody affinity purification to the STS1 recombinant protein using magnetic beads from Invitrogen (Chuck et al., 2014). Validation of antibody was performed by immunoblotting with total protein extract from *sts1* complemented lines and *sts1* mutants as a negative control. Primary antibody was used at 1:2000 dilution and secondary anti-guinea pig HRP-coupled antibody (Thermo Fisher Scientific catalog no. A18769) at 1:3000 dilution. STS1 immunolocalizations were performed as previously described by Chuck et al. (2010) and Tsuda and Chuck (2019). Primary antibody was used at 1:200 dilution and secondary anti-guinea pig alkaline phosphatase-coupled antibody (Thermo Fisher Scientific catalog no. A18772) at 1:300 dilution.

Anti-STS1, Anti-Ubiquitin, and pSer Immunoblots

SDS-PAGE with 12% (w/v) acrylamide gel was performed with 30 μg of protein extract from *sts1* and STS1-HET and STS1-HOM complemented mutants. Then, semidry transfer, blocking, and incubation with 1:2000 affinity-purified anti-STS1 guinea pig polyclonal antibody were performed. Protein was detected using chemiluminescence with 1:3000 anti-guinea pig secondary HRP-coupled antibody (Thermo Fisher Scientific catalog no. A18769). Membrane was stripped and tubulin was detected as a loading control by incubation with 1:25,000 mouse monoclonal anti-TUB DM1A (Abcam catalog no. ab7291). Detection was done using 1:10,000 anti-mouse secondary HRP-conjugated antibody (Amersham ECL GE catalog no. 45,001,275).

For measurement of STS1 protein level, after immunoblot images were captured by scanning of x-ray films, densitometry analysis was performed using ImageJ (1.4 NIH software; Schneider et al., 2012). The detailed protocol is described by Abraham-Juárez (2019). The relative abundance of STS1 in each sample was calculated by dividing the densitometry value of STS1 protein with the respective loading control (α-Tubulin). Then, samples were normalized to STS1-HET to establish the fold change between them. Data are shown in Supplemental Table 5. Three replicates were done with similar results.

For the phosphorylation and ubiquitination assays, STS1-YFP HET and HOM IPs were performed with anti-GFP antibody as described for IP above; PhosSTOP (Roche) was added to the protein extraction buffer for the phosphorylation assay. Based on previous densitometry experiments we performed to estimate the amount of protein in the two samples, 3 μL of the STS1-HOM and 9 μL of the STS1-HET IP elutions were loaded on two different gels (one for anti-pSer and one for anti-ubiquitin blot). Blocking was performed with 2% (w/v) BSA. For the phosphorylation assay, primary anti-pSer 16B4 mouse monoclonal antibody (Santa Cruz Biotechnology catalog no. sc-81514) was used at 1:1000; secondary anti-mouse HRP-conjugated antibody (Amersham ECL GE) was used at 1:3000. For the ubiquitination assay, primary anti-ubiquitin P4D1 mouse monoclonal antibody (Santa Cruz Biotechnology catalog no. sc-8017) was used at 1:1000 dilution and the same secondary anti-mouse antibody as used before at 1:3000. For development, Clarity ECL reagents (Bio-Rad) and the Azure c-300 Chemiluminescent Immunoblot Imaging System (Azure Biosystems) were used. After development, anti-pSer and anti-ubiquitin blots were stripped, blocked, and incubated with anti-GFP antibody (Mouse IgG1K, clones 7.1 and 13.1; Roche catalog no. 11814460001) at 1:1000 dilution and the same secondary anti-mouse antibody as used before at 1:3000. All immunoblots were repeated three times.

In Situ Hybridization

sts1 and *sts1* complemented inflorescences were fixed overnight at 4°C in 4% (w/v) paraformaldehyde in 1× PBS. Fixed samples were dehydrated in an ethanol series and transferred into Histoclear, then embedded in Paraplast, sectioned, and hybridized according to Bartlett et al. (2015).

RT-qPCR

Total RNA was isolated from 1.8-cm tassels using Trizol reagent according to the manufacturer's instructions. cDNA was synthesized using 1 μg of RNA, Oligo dT(20), and SSIII RT Reverse Transcriptase (Invitrogen) according to the manufacturer's instructions, for three independent biological replicates. qPCR was performed for each cDNA replicate and samples were run in duplicate, using the SYBR Green PCR master mix (Thermo Fisher Scientific). Cycling was done with the following conditions: 95°C for 10 min, 40 cycles of 95°C for 15 s and 60°C for 1 min, and a final melt curve stage from 60 to 95°C, in a StepOne system (Applied Biosystems). Data were normalized using *Actin* as the reference gene. To get fold change values, the $2^{-\Delta\Delta CT}$ method was used.

Accession Numbers

Raw sequencing data are available at the National Center for Biotechnology Information Sequence Read Archive (Bioproject PRJNA625570). Supplemental data sets and anther images are available at dryad (https://datadryad.org/stash/dataset/doi:10.5061/dryad.4xgxd2573). Code for analyses and figure generation is available on GitHub (https://github.com/BartlettLab/B-class).

Supplemental Data

Supplemental Figure 1. STS1 immunolocalizations and *in situ* hybridizations.

Supplemental Figure 2. Morphospace occupied by *STS1-HET* vs. *STS1-HOM* anthers.

Supplemental Table 1. Floral organ counts.

Supplemental Table 2. MADS-box proteins and chromatin remodelers identified in IP-MS experiments.

Supplemental Table 3. Kinases identified in IP-MS experiments.

Supplemental Table 4. Kinases identified in IP-MS experiments.

Supplemental Table 5. Ubiquitination machinery identified in IP-MS experiments.

Supplemental Table 6. Primers for genotyping assays and RT-qPCR.

Supplemental Table 7. Results of statistical tests.

Supplemental Data Set 1. Anther dimensions early in floral development.

Supplemental Data Set 2. Anther dimensions at anthesis.

Supplemental Data Set 3. Genes differentially expressed in STS1-HET vs sts1 mutant siblings.

Supplemental Data Set 4. Genes differentially expressed in STS1-HOM vs sts1 mutant siblings.

Supplemental Data Set 5. Genes differentially expressed in STS1-HET vs si1 mutant siblings.

Supplemental Data Set 6. Genes differentially expressed in STS1-HOM vs si1 mutant siblings.

Supplemental Data Set 7. Enriched GO-terms differentially expressed in STS1-HET vs sts1 mutant siblings.

Supplemental Data Set 8. Enriched GO-terms differentially expressed in STS1-HOM vs sts1 mutant siblings.

Supplemental Data Set 9. STS1-HET IP-MS two replicates IBAQ.

Supplemental Data Set 10. STS1-HOM IP-MS two replicates IBAQ.

Supplemental Data Set 11. Enriched GO-terms in proteins immunoprecipitated with STS1-HET.

Supplemental Data Set 12. Enriched GO-terms in proteins immunoprecipitated with STS1-HOM.

ACKNOWLEDGMENTS

We thank Ravi Ranjan at the Institute for Applied Life Sciences Genomics Resource Laboratory and James Chambers at the Institute for Applied Life Sciences LightMicroscopy Facility and Nikon Center of Excellence. We thank Dan Jones, Chris Joyner, Chris Phillips, and Neal Woodard, greenhouse and farm staff, at the University of Massachusetts Amherst for essential help. We thank Amanda Dee, Joseph Gallagher, Michelle Heeney, Jeff Heithmar, Harry Klein, Jamie Kostyun, Erin Patterson, and Grace Pisano, members of the Bartlett lab for help with lab work and for providing helpful comments on the article. We also thank Craig Albertson, Peter Chien, Lilian Fritz-Laylin, Joshua Gendron, David Jackson, Zachary Lippman, Michelle Facette, Eric Strieter, Beth Thompson, and three anonymous reviewers for helpful discussion and comments. This work was supported by the National Science Foundation (grants IOS-1652380 and IOS-1546837 to M.B.), the USDA National Institute of Food and Agriculture (grant NIFA-2018-67012-27998 to A.S.-L.), and the University of Massachusetts.

AUTHOR CONTRIBUTIONS

M.B., A.S.-L., M.J.A.-J., and C.W. designed the research; A.S.-L., M.J.A.-J., M.B., C.B., P.H., and J.M. conducted research and analyzed results; M.B., A.S.-L., and P.H. acquired funding for the research; M.B., M.J.A.-J., and A.S.-L. wrote the article with assistance from all coauthors.

Received April 16, 2020; revised August 19, 2020; accepted September 1, 2020; published September 1, 2020.

REFERENCES

Abraham-Juárez, M.J. (2019). Western blot in maize. Bio-101 e3257.

Adhvaryu, K.K., Gessaman, J.D., Honda, S., Lewis, Z.A., Grisafi, P.L., and Selker, E.U. (2015). The cullin-4 complex DCDC does not require E3 ubiquitin ligase elements to control heterochromatin in *Neurospora crassa*. Eukaryot. Cell **14:** 25–28.

Alhindi, T., Zhang, Z., Ruelens, P., Coenen, H., Degroote, H., Iraci, N., and Geuten, K. (2017). Protein interaction evolution from promiscuity to specificity with reduced flexibility in an increasingly complex network. Sci. Rep. **7:** 44948.

Ambrose, B.A., Lerner, D.R., Ciceri, P., Padilla, C.M., Yanofsky, M.F., and Schmidt, R.J. (2000). Molecular and genetic analyses of the silky1 gene reveal conservation in floral organ specification between eudicots and monocots. Mol. Cell **5:** 569–579.

Angenent, G.C., and Immink, R.G.H. (2009). Combinatorial action of petunia MADS box genes and their protein products. In Petunia: Evolutionary, Developmental and Physiological Genetics, T. Gerats, and and J. Strommer, eds (New York: Springer), pp. 225–245.

Ashman, T.L., and Majetic, C.J. (2006). Genetic constraints on floral evolution: A review and evaluation of patterns. Heredity **96:** 343–352.

Bartlett, M., Thompson, B., Brabazon, H., Del Gizzi, R., Zhang, T., and Whipple, C. (2016). Evolutionary dynamics of floral homeotic transcription factor protein-protein interactions. Mol. Biol. Evol. **33:** 1486–1501.

Bartlett, M.E. (2017). Changing MADS-box transcription factor protein-protein interactions as a mechanism for generating floral morphological diversity. Integr. Comp. Biol. **57:** 1312–1321.

Bartlett, M.E., and Specht, C.D. (2010). Evidence for the involvement of Globosa-like gene duplications and expression divergence in the evolution of floral morphology in the Zingiberales. New Phytol. **187:** 521–541.

Bartlett, M.E., Williams, S.K., Taylor, Z., DeBlasio, S., Goldshmidt, A., Hall, D.H., Schmidt, R.J., Jackson, D.P., and Whipple, C.J. (2015). The maize *PI/GLO* ortholog *Zmm16/sterile tassel silky ear1* interacts with the zygomorphy and sex determination pathways in flower development. Plant Cell **27:** 3081–3098.

Bergey, C.M., Lopez, M., Harrison, G.F., Patin, E., Cohen, J.A., Quintana-Murci, L., Barreiro, L.B., and Perry, G.H. (2018). Polygenic adaptation and convergent evolution on growth and cardiac genetic pathways in African and Asian rainforest hunter-gatherers. Proc. Natl. Acad. Sci. USA **115:** E11256–E11263.

Bezhani, S., Winter, C., Hershman, S., Wagner, J.D., Kennedy, J.F., Kwon, C.S., Pfluger, J., Su, Y., and Wagner, D. (2007). Unique, shared, and redundant roles for the Arabidopsis SWI/SNF chromatin remodeling ATPases BRAHMA and SPLAYED. Plant Cell **19:** 403–416.

Bonhomme, V., Picq, S., Gaucherel, C., and Claude, J. (2014). Momocs: Outline analysis using R. J. Stat. Softw. **56:** 1–24.

Buckler, E.S., Gaut, B.S., and McMullen, M.D. (2006). Molecular and functional diversity of maize. Curr. Opin. Plant Biol. **9:** 172–176.

Chang, L., Zhang, Z., Yang, J., McLaughlin, S.H., and Barford, D. (2015). Atomic structure of the APC/C and its mechanism of protein ubiquitination. Nature **522:** 450–454.

Chen, H., Shen, Y., Tang, X., Yu, L., Wang, J., Guo, L., Zhang, Y., Zhang, H., Feng, S., Strickland, E., Zheng, N., and Deng, X.W. (2006). Arabidopsis CULLIN4 forms an E3 ubiquitin ligase with RBX1 and the CDD complex in mediating light control of development. Plant Cell **18:** 1991–2004.

Chuck, G., Whipple, C., Jackson, D., and Hake, S. (2010). The maize SBP-box transcription factor encoded by tasselsheath4 regulates bract development and the establishment of meristem boundaries. Development **137:** 1243–1250.

Chuck, G.S., Brown, P.J., Meeley, R., and Hake, S. (2014). Maize SBP-box transcription factors unbranched2 and unbranched3 affect yield traits by regulating the rate of lateral primordia initiation. Proc. Natl. Acad. Sci. USA **111:** 18775–18780.

Citterio, S., Sgorbati, S., Levi, M., Colombo, B.M., and Sparvoli, E. (1992). PCNA and total nuclear protein content as markers of cell proliferation in pea tissue. J. Cell Sci. **102:** 71–78.

Clark, N.M., Fisher, A.P., Berckmans, B., Van den Broeck, L., Nelson, E.C., Nguyen, T.T., Bustillo-Avendaño, E., Zebell, S.G., Moreno-Risueno, M.A., Simon, R., Gallagher, K.L., and Sozzani, R. (2020). Protein complex stoichiometry and expression dynamics of transcription factors modulate stem cell division. Proc. Natl. Acad. Sci. USA **117:** 15332–15342.

Conner, J.K., Karoly, K., Stewart, C., Koelling, V.A., Sahli, H.F., and Shaw, F.H. (2011). Rapid independent trait evolution despite a strong pleiotropic genetic correlation. Am. Nat. **178:** 429–441.

Coppotelli, G., Mughal, N., Marescotti, D., and Masucci, M.G. (2011). High avidity binding to DNA protects ubiquitylated substrates from proteasomal degradation. J. Biol. Chem. **286:** 19565–19575.

Cui, M.-L., Copsey, L., Green, A.A., Bangham, J.A., and Coen, E. (2010). Quantitative control of organ shape by combinatorial gene activity. PLoS Biol. **8:** e1000538.

Davey, N.E., and Morgan, D.O. (2016). Building a regulatory network with short linear sequence motifs: Lessons from the degrons of the anaphase-promoting complex. Mol. Cell **64:** 12–23.

Ding, Y., Tang, Y., Kwok, C.K., Zhang, Y., Bevilacqua, P.C., and Assmann, S.M. (2014). In vivo genome-wide profiling of RNA secondary structure reveals novel regulatory features. Nature **505:** 696–700.

Dobin, A., Davis, C.A., Schlesinger, F., Drenkow, J., Zaleski, C., Jha, S., Batut, P., Chaisson, M., and Gingeras, T.R. (2013). STAR: Ultrafast universal RNA-seq aligner. Bioinformatics **29:** 15–21.

Duan, E., et al. (2019). OsSHI1 regulates plant architecture through modulating the transcriptional activity of IPA1 in rice. Plant Cell **31:** 1026–1042.

Ella, H., Reiss, Y., and Ravid, T. (2019). The hunt for degrons of the 26S proteasome. Biomolecules **9:** 230.

Endress, P.K. (1992). Evolution and floral diversity: The phylogenetic surroundings of Arabidopsis and Antirrhinum. Int. J. Plant Sci. **153:** S106–S122.

Feng, S., Shen, Y., Sullivan, J.A., Rubio, V., Xiong, Y., Sun, T.-P., and Deng, X.W. (2004). Arabidopsis CAND1, an unmodified CUL1-interacting protein, is involved in multiple developmental pathways controlled by ubiquitin/proteasome-mediated protein degradation. Plant Cell **16:** 1870–1882.

Fobert, P.R., Coen, E.S., Murphy, G.J., and Doonan, J.H. (1994). Patterns of cell division revealed by transcriptional regulation of genes during the cell cycle in plants. EMBO J. **13:** 616–624.

Fujita, H., Takemura, M., Tani, E., Nemoto, K., Yokota, A., and Kohchi, T. (2003). An Arabidopsis MADS-box protein, AGL24, is specifically bound to and phosphorylated by meristematic receptor-like kinase (MRLK). Plant Cell Physiol. **44:** 735–742.

Gao, J., Thelen, J.J., Dunker, A.K., and Xu, D. (2010). Musite, a tool for global prediction of general and kinase-specific phosphorylation sites. Mol. Cell. Proteomics **9:** 2586–2600.

Geffen, Y., Appleboim, A., Gardner, R.G., Friedman, N., Sadeh, R., and Ravid, T. (2016). Mapping the landscape of a eukaryotic degronome. Mol. Cell **63:** 1055–1065.

Geuten, K., and Irish, V. (2010). Hidden variability of floral homeotic B genes in Solanaceae provides a molecular basis for the evolution of novel functions. Plant Cell **22:** 2562–2578.

Gingold, H., and Pilpel, Y. (2011). Determinants of translation efficiency and accuracy. Mol. Syst. Biol. **7:** 481.

Gomariz-Fernández, A., Sánchez-Gerschon, V., Fourquin, C., and Ferrándiz, C. (2017). The role of *SHI/STY/SRS* genes in organ growth and carpel development is conserved in the distant eudicot species *Arabidopsis thaliana* and *Nicotiana benthamiana*. Front. Plant Sci. **8:** 814.

Goto, K., and Meyerowitz, E.M. (1994). Function and regulation of the Arabidopsis floral homeotic gene PISTILLATA. Genes Dev. **8:** 1548–1560.

He, B., Shi, J., Wang, X., Jiang, H., and Zhu, H.-J. (2019). Label-free absolute protein quantification with data-independent acquisition. J. Proteomics **200:** 51–59.

Hickey, C.M., Xie, Y., and Hochstrasser, M. (2018). DNA binding by the MATα2 transcription factor controls its access to alternative ubiquitin-modification pathways. Mol. Biol. Cell **29:** 542–556.

Hileman, L.C., and Irish, V.F. (2009). More is better: The uses of developmental genetic data to reconstruct perianth evolution. Am. J. Bot. **96:** 83–95.

Honma, T., and Goto, K. (2001). Complexes of MADS-box proteins are sufficient to convert leaves into floral organs. Nature **409:** 525–529.

Hsu, H.-F., Hsu, W.-H., Lee, Y.-I., Mao, W.-T., Yang, J.-Y., Li, J.-Y., and Yang, C.-H. (2015). Model for perianth formation in orchids. Nat. Plants **1:** 15046.

Hu, X., Kong, X., Wang, C., Ma, L., Zhao, J., Wei, J., Zhang, X., Loake, G.J., Zhang, T., Huang, J., and Yang, Y. (2014). Proteasome-mediated degradation of FRIGIDA modulates flowering time in Arabidopsis during vernalization. Plant Cell **26:** 4763–4781.

Hugouvieux, V., Silva, C.S., Jourdain, A., Stigliani, A., Charras, Q., Conn, V., Conn, S.J., Carles, C.C., Parcy, F., and Zubieta, C. (2018). Tetramerization of MADS family transcription factors SEPALLATA3 and AGAMOUS is required for floral meristem determinacy in Arabidopsis. Nucleic Acids Res. **46:** 4966–4977.

Jack, T., Brockman, L.L., and Meyerowitz, E.M. (1992). The homeotic gene APETALA3 of *Arabidopsis thaliana* encodes a MADS box and is expressed in petals and stamens. Cell **68:** 683–697.

Jiao, Y., et al. (2017). Improved maize reference genome with single-molecule technologies. Nature **546:** 524–527.

Johnson, P.R., Swanson, R., Rakhilina, L., and Hochstrasser, M. (1998). Degradation signal masking by heterodimerization of MATα2 and MATa1 blocks their mutual destruction by the ubiquitin-proteasome pathway. Cell **94:** 217–227.

Jorrín-Novo, J.V., Pascual, J., Sánchez-Lucas, R., Romero-Rodríguez, M.C., Rodríguez-Ortega, M.J., Lenz, C., and Valledor, L. (2015). Fourteen years of plant proteomics reflected in Proteomics: Moving from model species and 2DE-based approaches to orphan species and gel-free platforms. Proteomics **15:** 1089–1112.

Kim, S., Koh, J., Yoo, M.-J., Kong, H., Hu, Y., Ma, H., Soltis, P.S., and Soltis, D.E. (2005). Expression of floral MADS-box genes in basal angiosperms: Implications for the evolution of floral regulators. Plant J. **43:** 724–744.

Kiparaki, M., Zarifi, I., and Delidakis, C. (2015). bHLH proteins involved in Drosophila neurogenesis are mutually regulated at the level of stability. Nucleic Acids Res. **43:** 2543–2559.

Kramer, E.M., Holappa, L., Gould, B., Jaramillo, M.A., Setnikov, D., and Santiago, P.M. (2007). Elaboration of B gene function to include the identity of novel floral organs in the lower eudicot Aquilegia. Plant Cell **19:** 750–766.

Krey, J.F., Wilmarth, P.A., Shin, J.-B., Klimek, J., Sherman, N.E., Jeffery, E.D., Choi, D., David, L.L., and Barr-Gillespie, P.G. (2014). Accurate label-free protein quantitation with high- and low-resolution mass spectrometers. J. Proteome Res. **13:** 1034–1044.

Krizek, B.A., and Fletcher, J.C. (2005). Molecular mechanisms of flower development: An armchair guide. Nat. Rev. Genet. **6:** 688–698.

Kudla, G., Murray, A.W., Tollervey, D., and Plotkin, J.B. (2009). Coding-sequence determinants of gene expression in *Escherichia coli*. Science **324:** 255–258.

Kuusk, S., Sohlberg, J.J., Magnus Eklund, D., and Sundberg, E. (2006). Functionally redundant SHI family genes regulate Arabidopsis gynoecium development in a dose-dependent manner. Plant J. **47:** 99–111.

Landberg, K., Pederson, E.R.A., Viaene, T., Bozorg, B., Friml, J., Jönsson, H., Thelander, M., and Sundberg, E. (2013). The moss *Physcomitrella patens* reproductive organ development is highly organized, affected by the two SHI/STY genes and by the level of active auxin in the SHI/STY expression domain. Plant Physiol. **162:** 1406–1419.

Li, C., Chen, C., Gao, L., Yang, S., Nguyen, V., Shi, X., Siminovitch, K., Kohalmi, S.E., Huang, S., Wu, K., Chen, X., and Cui, Y. (2015). The Arabidopsis SWI2/SNF2 chromatin remodeler BRAHMA regulates polycomb function during vegetative development and directly activates the flowering repressor gene SVP. PLoS Genet. **11:** e1004944.

Li, J., Cocker, J.M., Wright, J., Webster, M.A., McMullan, M., Dyer, S., Swarbreck, D., Caccamo, M., Oosterhout, C.V., and Gilmartin, P.M. (2016). Genetic architecture and evolution of the S locus supergene in *Primula vulgaris*. Nat. Plants **2:** 16188.

Litt, A., and Kramer, E.M. (2010). The ABC model and the diversification of floral organ identity. Semin. Cell Dev. Biol. **21:** 129–137.

Liu, C., Xi, W., Shen, L., Tan, C., and Yu, H. (2009). Regulation of floral patterning by flowering time genes. Dev. Cell **16:** 711–722.

Lu, Z., and Hunter, T. (2018). Metabolic kinases moonlighting as protein kinases. Trends Biochem. Sci. **43:** 301–310.

MacLean, A.M., Orlovskis, Z., Kowitwanich, K., Zdziarska, A.M., Angenent, G.C., Immink, R.G.H., and Hogenhout, S.A. (2014). Phytoplasma effector SAP54 hijacks plant reproduction by degrading MADS-box proteins and promotes insect colonization in a RAD23-dependent manner. PLoS Biol. **12:** e1001835.

Manzano, C., Abraham, Z., López-Torrejón, G., and Del Pozo, J.C. (2008). Identification of ubiquitinated proteins in Arabidopsis. Plant Mol. Biol. **68:** 145–158.

Masiero, S., Imbriano, C., Ravasio, F., Favaro, R., Pelucchi, N., Gorla, M.S., Mantovani, R., Colombo, L., and Kater, M.M. (2002). Ternary complex formation between MADS-box transcription factors and the histone fold protein NF-YB. J. Biol. Chem. **277:** 26429–26435.

McCarthy, D.J., Chen, Y., and Smyth, G.K. (2012). Differential expression analysis of multifactor RNA-seq experiments with respect to biological variation. Nucleic Acids Res. **40:** 4288–4297.

Melzer, R., Härter, A., Rümpler, F., Kim, S., Soltis, P.S., Soltis, D.E., and Theißen, G. (2014). DEF- and GLO-like proteins may have lost most of their interaction partners during angiosperm evolution. Ann. Bot. **114:** 1431–1443.

Millar, A.H., Heazlewood, J.L., Giglione, C., Holdsworth, M.J., Bachmair, A., and Schulze, W.X. (2019). The scope, functions, and dynamics of posttranslational protein modifications. Annu. Rev. Plant Biol. **70:** 119–151.

Min, Y., Bunn, J.I., and Kramer, E.M. (2019). Homologs of the STYLISH gene family control nectary development in Aquilegia. New Phytol. **221:** 1090–1100.

Molkentin, J.D., Li, L., and Olson, E.N. (1996). Phosphorylation of the MADS-box transcription factor MEF2C enhances its DNA binding activity. J. Biol. Chem. **271:** 17199–17204.

Mondragón-Palomino, M., and Theissen, G. (2008). MADS about the evolution of orchid flowers. Trends Plant Sci. **13:** 51–59.

Mondragón-Palomino, M., and Theissen, G. (2009). Why are orchid flowers so diverse? Reduction of evolutionary constraints by paralogues of class B floral homeotic genes. Ann. Bot. **104:** 583–594.

Mondragón-Palomino, M., and Theissen, G. (2011). Conserved differential expression of paralogous DEFICIENS- and GLOBOSA-like MADS-box genes in the flowers of Orchidaceae: Refining the 'orchid code'. Plant J. **66:** 1008–1019.

Moss, B.L., Mao, H., Guseman, J.M., Hinds, T.R., Hellmuth, A., Kovenock, M., Noorassa, A., Lanctot, A., Villalobos, L.I.A.C., Zheng, N., and Nemhauser, J.L. (2015). Rate motifs tune auxin/indole-3-acetic acid degradation dynamics. Plant Physiol. **169:** 803–813.

Münster, T., Deleu, W., Wingen, L.U., Ouzunova, M., Cacharrón, J., Faigl, W., Werth, S., Kim, J.T.T., Saedler, H., and Theißen, G. (2002). Maize MADS-box genes galore. Maydica **47:** 287–301.

Opanowicz, M., Vain, P., Draper, J., Parker, D., and Doonan, J.H. (2008). *Brachypodium distachyon*: Making hay with a wild grass. Trends Plant Sci. **13:** 172–177.

Opedal, Ø.H. (2019). The evolvability of animal-pollinated flowers: Towards predicting adaptation to novel pollinator communities. New Phytol. **221:** 1128–1135.

Opedal, Ø.H., Bolstad, G.H., Hansen, T.F., Armbruster, W.S., and Pélabon, C. (2017). The evolvability of herkogamy: Quantifying the evolutionary potential of a composite trait. Evolution **71:** 1572–1586.

Patharkar, O.R., and Walker, J.C. (2016). Core mechanisms regulating developmentally timed and environmentally triggered abscission. Plant Physiol. **172:** 510–520.

Radivojac, P., Vacic, V., Haynes, C., Cocklin, R.R., Mohan, A., Heyen, J.W., Goebl, M.G., and Iakoucheva, L.M. (2010). Identification, analysis, and prediction of protein ubiquitination sites. Proteins **78:** 365–380.

Risso, D., Ngai, J., Speed, T.P., and Dudoit, S. (2014). Normalization of RNA-seq data using factor analysis of control genes or samples. Nat. Biotechnol. **32:** 896–902.

Robinson, M.D., McCarthy, D.J., and Smyth, G.K. (2010). edgeR: A Bioconductor package for differential expression analysis of digital gene expression data. Bioinformatics **26:** 139–140.

Rosa-Téllez, S., Anoman, A.D., Flores-Tornero, M., Toujani, W., Alseek, S., Fernie, A.R., Nebauer, S.G., Muñoz-Bertomeu, J., Segura, J., and Ros, R. (2018). Phosphoglycerate kinases are co-regulated to adjust metabolism and to optimize growth. Plant Physiol. **176:** 1182–1198.

Rudall, P.J., and Bateman, R.M. (2004). Evolution of zygomorphy in monocot flowers: Iterative patterns and developmental constraints. New Phytol. **162:** 25–44.

Ruelens, P., Zhang, Z., van Mourik, H., Maere, S., Kaufmann, K., and Geuten, K. (2017). The origin of floral organ identity quartets. Plant Cell **29:** 229–242.

Sang, Y., Silva-Ortega, C.O., Wu, S., Yamaguchi, N., Wu, M.-F., Pfluger, J., Gillmor, C.S., Gallagher, K.L., and Wagner, D. (2012). Mutations in two non-canonical Arabidopsis SWI2/SNF2 chromatin remodeling ATPases cause embryogenesis and stem cell maintenance defects. Plant J. **72:** 1000–1014.

Schneider, C.A., Rasband, W.S., and Eliceiri, K.W. (2012). NIH Image to ImageJ: 25 years of image analysis. Nat. Methods **9:** 671–675.

Schrader, E.K., Harstad, K.G., and Matouschek, A. (2009). Targeting proteins for degradation. Nat. Chem. Biol. **5:** 815–822.

Sharma, B., and Kramer, E.M. (2017). *Aquilegia* B gene homologs promote petaloidy of the sepals and maintenance of the C domain boundary. Evodevo **8:** 22.

Silva, C.S., Puranik, S., Round, A., Brennich, M., Jourdain, A., Parcy, F., Hugouvieux, V., and Zubieta, C. (2016). Evolution of the plant reproduction master regulators LFY and the MADS transcription factors: The role of protein structure in the evolutionary development of the flower. Front. Plant Sci. **6:** 1193.

Sinitcyn, P., Rudolph, J.D., and Cox, J. (2018). Computational methods for understanding mass spectrometry-based shotgun proteomics data. Annu. Rev. Biomed. Data Sci. **1:** 207–234.

Smaczniak, C., et al. (2012). Characterization of MADS-domain transcription factor complexes in Arabidopsis flower development. Proc. Natl. Acad. Sci. USA **109:** 1560–1565.

Tang, W., Kim, T.W., Oses-Prieto, J.A., Sun, Y., Deng, Z., Zhu, S., Wang, R., Burlingame, A.L., and Wang, Z.Y. (2008). BSKs mediate signal transduction from the receptor kinase BRI1 in Arabidopsis. Science **321:** 557–560.

Theissen, G., Melzer, R., and Rümpler, F. (2016). MADS-domain transcription factors and the floral quartet model of flower development: Linking plant development and evolution. Development **143:** 3259–3271.

Theissen, G., and Saedler, H. (2001). Plant biology: Floral quartets. Nature **409:** 469–471.

Thouly, C., Le Masson, M., Lai, X., Carles, C.C., and Vachon, G. (2020). Unwinding BRAHMA functions in plants. Genes (Basel) **11:** 90.

Timerman, D., and Barrett, S.C.H. (2019). Comparative analysis of pollen release biomechanics in Thalictrum: Implications for evolutionary transitions between animal and wind pollination. New Phytol. **224:** 1121–1132.

Timerman, D., Greene, D.F., Urzay, J., and Ackerman, J.D. (2014). Turbulence-induced resonance vibrations cause pollen release in wind-pollinated *Plantago lanceolata* L. (Plantaginaceae). J. R. Soc. Interface **11:** 20140866.

Tsuda, K., and Chuck, G. (2019). Heat induced epitope retrieval (HIER) assisted protein immunostaining in maize. Bio-101 9.

Tuller, T., Carmi, A., Vestsigian, K., Navon, S., Dorfan, Y., Zaborske, J., Pan, T., Dahan, O., Furman, I., and Pilpel, Y. (2010). An evolutionarily conserved mechanism for controlling the efficiency of protein translation. Cell **141:** 344–354.

Tzeng, T.-Y., Kong, L.-R., Chen, C.-H., Shaw, C.-C., and Yang, C.-H. (2009). Overexpression of the lily p70(s6k) gene in Arabidopsis affects elongation of flower organs and indicates TOR-dependent regulation of AP3, PI and SUP translation. Plant Cell Physiol. **50:** 1695–1709.

Vachon, G., Engelhorn, J., and Carles, C.C. (2018). Interactions between transcription factors and chromatin regulators in the control of flower development. J. Exp. Bot. **69:** 2461–2471.

Vandenbussche, M., Zethof, J., Royaert, S., Weterings, K., and Gerats, T. (2004). The duplicated B-class heterodimer model: Whorl-specific effects and complex genetic interactions in *Petunia hybrida* flower development. Plant Cell **16:** 741–754.

Verma, M., Choi, J., Cottrell, K.A., Lavagnino, Z., Thomas, E.N., Pavlovic-Djuranovic, S., Szczesny, P., Piston, D.W., Zaher, H.S., Puglisi, J.D., and Djuranovic, S. (2019). A short translational ramp determines the efficiency of protein synthesis. Nat. Commun. **10:** 5774.

Veron, A.S., Kaufmann, K., and Bornberg-Bauer, E. (2007). Evidence of interaction network evolution by whole-genome duplications: A case study in MADS-box proteins. Mol. Biol. Evol. **24:** 670–678.

Wagner, A. (2012). The role of robustness in phenotypic adaptation and innovation. Proc. Biol. Sci. **279:** 1249–1258.

Wang, J., et al. (2018). A single transcription factor promotes both yield and immunity in rice. Science **361:** 1026–1028.

Wang, Y., Hou, Y., Gu, H., Kang, D., Chen, Z., Liu, J., and Qu, L.J. (2012). The Arabidopsis APC4 subunit of the anaphase-promoting complex/cyclosome (APC/C) is critical for both female gametogenesis and embryogenesis. Plant J. **69:** 227–240.

Wang, Y., Hou, Y., Gu, H., Kang, D., Chen, Z.-L., Liu, J., and Qu, L.-J. (2013). The Arabidopsis anaphase-promoting complex/cyclosome subunit 1 is critical for both female gametogenesis and embryogenesis. J. Integr. Plant Biol. **55:** 64–74.

Wang, Y.-Q., Melzer, R., and Theissen, G. (2010). Molecular interactions of orthologues of floral homeotic proteins from the gymnosperm *Gnetum gnemon* provide a clue to the evolutionary origin of 'floral quartets'. Plant J. **64:** 177–190.

Wei, B., Zhang, R.-Z., Guo, J.-J., Liu, D.-M., Li, A.-L., Fan, R.-C., Mao, L., and Zhang, X.-Q. (2014). Genome-wide analysis of the MADS-box gene family in *Brachypodium distachyon*. PLoS One **9:** e84781.

Wertz, I.E., O'Rourke, K.M., Zhang, Z., Dornan, D., Arnott, D., Deshaies, R.J., and Dixit, V.M. (2004). Human De-etiolated-1 regulates c-Jun by assembling a CUL4A ubiquitin ligase. Science **303:** 1371–1374.

Whipple, C.J., Ciceri, P., Padilla, C.M., Ambrose, B.A., Bandong, S.L., and Schmidt, R.J. (2004). Conservation of B-class floral homeotic gene function between maize and Arabidopsis. Development **131:** 6083–6091.

Wimalanathan, K., Friedberg, I., Andorf, C.M., and Lawrence-Dill, C.J. (2018). Maize GO annotation: Methods, evaluation, and review (maize-GAMER). Plant Direct **2:** e00052.

Wu, M.-F., Sang, Y., Bezhani, S., Yamaguchi, N., Han, S.-K., Li, Z., Su, Y., Slewinski, T.L., and Wagner, D. (2012). SWI2/SNF2 chromatin remodeling ATPases overcome polycomb repression and control floral organ identity with the LEAFY and SEPALLATA3 transcription factors. Proc. Natl. Acad. Sci. USA **109:** 3576–3581.

Wuest, S.E., O'Maoileidigh, D.S., Rae, L., Kwasniewska, K., Raganelli, A., Hanczaryk, K., Lohan, A.J., Loftus, B., Graciet, E., and Wellmer, F. (2012). Molecular basis for the specification of floral organs by APETALA3 and PISTILLATA. Proc. Natl. Acad. Sci. USA **109:** 13452–13457.

Xu, P., Xu, S.-L., Li, Z.-J., Tang, W., Burlingame, A.L., and Wang, Z.-Y. (2014). A brassinosteroid-signaling kinase interacts with multiple receptor-like kinases in Arabidopsis. Mol. Plant **7:** 441–444.

Xu, R.Y., Xu, J., Wang, L., Niu, B., Copenhaver, G.P., Ma, H., Zheng, B., and Wang, Y. (2019). The Arabidopsis anaphase-promoting complex/cyclosome subunit 8 is required for male meiosis. New Phytol. **224:** 229–241.

Xu, X., Zhu, T., Nikonorova, N., and De Smet, I. (2018). Phosphorylation-mediated signalling in plants. Annual Plant Reviews Online **2:** 909–932.

Yang, Y., Fanning, L., and Jack, T. (2003). The K domain mediates heterodimerization of the Arabidopsis floral organ identity proteins, APETALA3 and PISTILLATA. Plant J. **33:** 47–59.

Yao, Q., Gao, J., Bollinger, C., Thelen, J.J., and Xu, D. (2012). Predicting and analyzing protein phosphorylation sites in plants using Musite. Front. Plant Sci. **3:** 186.

Young, M.D., Wakefield, M.J., Smyth, G.K., and Oshlack, A. (2010). Gene Ontology analysis for RNA-seq: Accounting for selection bias. Genome Biol. **11:** R14.

Youssef, H.M., et al. (2017). VRS2 regulates hormone-mediated inflorescence patterning in barley. Nat. Genet. **49:** 157–161.

Yuo, T., Yamashita, Y., Kanamori, H., Matsumoto, T., Lundqvist, U., Sato, K., Ichii, M., Jobling, S.A., and Taketa, S. (2012). A SHORT INTERNODES (SHI) family transcription factor gene regulates awn elongation and pistil morphology in barley. J. Exp. Bot. **63:** 5223–5232.

Zahn, L.M., Kong, H., Leebens-Mack, J.H., Kim, S., Soltis, P.S., Landherr, L.L., Soltis, D.E., Depamphilis, C.W., and Ma, H. (2005). The evolution of the SEPALLATA subfamily of MADS-box

genes: A preangiosperm origin with multiple duplications throughout angiosperm history. Genetics **169:** 2209–2223.

Zhang, Z., Coenen, H., Ruelens, P., Hazarika, R.R., Al Hindi, T., Oguis, G.K., Vandeperre, A., van Noort, V., and Geuten, K. (2018). Resurrected protein interaction networks reveal the innovation potential of ancient whole-genome duplication. Plant Cell **30:** 2741–2760.

Zhu, S.-Y., et al. (2007). Two calcium-dependent protein kinases, CPK4 and CPK11, regulate abscisic acid signal transduction in Arabidopsis. Plant Cell **19:** 3019–3036.